Geosci. Model Dev. Discuss., 8, 9859–9924, 2015
www.geosci-model-dev-discuss.net/8/9859/2015/
doi:10.5194/gmdd-8-9859-2015

Geoscientific Model Development Discussions
Open Access
EGU

Experimental design for three interrelated Marine Ice-Sheet and Ocean Model Intercomparison Projects

X. S. Asay-Davis[1], S. L. Cornford[2], G. Durand[3,4], B. K. Galton-Fenzi[5,6], R. M. Gladstone[6,7], G. H. Gudmundsson[8], T. Hattermann[9,10], D. M. Holland[11], D. Holland[12], P. R. Holland[8], D. F. Martin[13], P. Mathiot[8,14], F. Pattyn[15], and H. Seroussi[16]

[1]Earth System Analysis, Potsdam Institute for Climate Impact Research, Potsdam, Germany
[2]Centre for Polar Observation and Modelling, University of Bristol, Bristol, UK
[3]CNRS, LGGE, 38041 Grenoble, France
[4]Univ. Grenoble Alpes, LGGE, 38041 Grenoble, France
[5]Australian Antarctic Division, Kingston, Tasmania, Australia
[6]Antarctic Climate and Ecosystems Cooperative Research Centre, Hobart, Tasmania, Australia
[7]Versuchsanstalt für Wasserbau, Hydrologie und Glaziologie (VAW), ETH Zurich, Switzerland
[8]British Antarctic Survey, Cambridge, UK
[9]Akvaplan-niva, Tromsø, Norway

[10]Alfred Wegener Institute, Helmholtz Centre for Polar and Marine Research, Bremerhaven, Germany
[11]Courant Institute of Mathematical Sciences, New York University, New York, NY, USA
[12]Center for Global Sea Level Change, New York University Abu Dhabi, Abu Dhabi, UAE
[13]Lawrence Berkeley National Laboratory, Berkeley, CA, USA
[14]Met Office, Exeter, UK
[15]Laboratoire de Glaciologie, Université Libre de Bruxelles, Brussels, Belgium
[16]Jet Propulsion Laboratory, California Institute of Technology, Pasadena, CA, USA

Received: 4 October 2015 – Accepted: 29 October 2015 – Published: 11 November 2015

Correspondence to: X. S. Asay-Davis (xylar.asay-davis@pik-potsdam.de)

Published by Copernicus Publications on behalf of the European Geosciences Union.

GMDD
8, 9859–9924, 2015

Abstract

Coupled ice sheet-ocean models capable of simulating moving grounding lines are just becoming available. Such models have a broad range of potential applications in studying the dynamics of marine ice sheets and tidewater glaciers, from process studies to future projections of ice mass loss and sea level rise. The Marine Ice Sheet-Ocean Model Intercomparison Project (MISOMIP) is a community effort aimed at designing and coordinating a series of model intercomparison projects (MIPs) for model evaluation in idealized setups, model verification based on observations, and future projections for key regions in the West Antarctic Ice Sheet (WAIS).

Here we describe computational experiments constituting three interrelated MIPs for marine ice sheet models and regional ocean circulation models incorporating ice shelf cavities. These consist of ice sheet experiments under the Marine Ice Sheet MIP third phase (MISMIP+), ocean experiments under the ice shelf-ocean MIP second phase (ISOMIP+) and coupled ice sheet-ocean experiments under the MISOMIP first phase (MISOMIP1). All three MIPs use a shared domain with idealized bedrock topography and forcing, allowing the coupled simulations (MISOMIP1) to be compared directly to the individual component simulations (MISMIP+ and ISOMIP+). The experiments, which have qualitative similarities to Pine Island Glacier Ice Shelf and the adjacent region of the Amundsen Sea, are designed to explore the effects of changes in ocean conditions, specifically the temperature at depth, on basal melting and ice dynamics. In future work, differences between model results will form the basis for evaluation of the participating models.

1 Introduction

The Marine Ice Sheet-Ocean Model Intercomparison Project (MISOMIP) is a targeted activity of the World Climate Research Programme's Climate and Cryosphere (CliC) project. MISOMIP is a community effort aimed at better quantifying sea-level change

GMDD
8, 9859–9924, 2015

induced by increased mass loss from the West Antarctic Ice Sheet (WAIS), particularly the Amundsen Sea region. At the first MISOMIP workshop held at New York University, Abu Dhabi in October 2014, participants decided that intercomparisons of ice sheet-ocean dynamics in realistic configurations would be more credible if it was preceded by a more idealized intercomparison and evaluation process for the standalone components and coupled models involved. While MISOMIP's longer-term goal is to investigate WAIS, we felt that the idealized MIPs would be applicable to a wide variety of models used to investigate a number of processes related to ice sheet and glacier interactions with the ocean. In addition to model evaluation, these idealized MIPs should be designed as a framework for exploring and comparing emergent properties of the coupled system.

1.1 Marine Ice Sheet Model Intercomparsion Projects (MISMIPs)

At the time of the workshop, two previous Model Intercomparison Projects (MIPs) focused on verifying and evaluating standalone ice-sheet models for marine ice sheets had taken place and a third was under development. The first MISMIP (Pattyn et al., 2012) compared the grounding-line dynamics between 14 models with a total of 27 unique configurations, and with a semi-analytic solution (Schoof, 2007a, b). The MISMIP experiments were designed for flowline models in which topography and other model fields varied in only one horizontal dimension (1HD). Within each experiment, a parameter (the ice softness) was varied through a series of discrete values, leading to advance and subsequent retreat of the grounding line. At each stage of the advance and retreat cycle, the model was allowed to reach steady state, typically over timescales of thousands to tens of thousands of years. The results showed that steady-state grounding-line positions could differ markedly depending on the resolution, type of stress approximation, and discretization methods employed. Comparison between the semi-analytic solution and high-resolution models with adaptive grids allowed the community to assess which model configurations gave accurate results and which configurations were likely not appropriate for marine ice-sheet studies. An important finding

GMDD
8, 9859–9924, 2015

of MISMIP related studies (Durand et al., 2009; Gladstone et al., 2010; Cornford et al., 2013) was that models with fixed grids (as opposed to those that track the grounding line in time) and without sub-grid-scale parameterizations of the grounding line require grounding-line resolution on the order of hundreds of meters to accurately reproduce grounding-line dynamics.

The second ice-sheet MIP, MISMIP3d (Pattyn et al., 2013), aimed at exploring grounding-line dynamics on centennial timescales in a configuration that varied in two horizontal dimensions (2HD). Dynamics were induced through a perturbation in the basal slipperiness in the center of the domain near the grounding line. MISMIP3d also tested the reversibility of the grounding-line position once the perturbation was removed. Results from 16 models with a total of 33 unique configurations showed that initial steady states as well as the reversibility of the dynamics differed significantly depending on the stress approximation and horizontal resolution.

Both MISMIP and MISMIP3d provided a basis for a number of follow-up studies focused on both improvements in numerical methods (e.g. Drouet et al., 2013; Leguy et al., 2014; Feldmann et al., 2014; Seroussi et al., 2014b) and exploring changes in the model topography and physics parameterizations (e.g. Leguy et al., 2014; Feldmann and Levermann, 2015; Tsai et al., 2015).

The third marine ice-sheet MIP (MISMIP+), described in Sect. 2, examines marine ice-sheet dynamics in 2HD with strong buttressing. An idealized bedrock topoography, based on the work of Gudmundsson et al. (2012) and Gudmundsson (2013), was designed to produce a steady state featuring a grounding line lying partly on a retrograde slope in the absence of ice shelf melt. The three major MISMIP+ experiments prescribe melt rates varying from no melt in a control experiment, to strong melt rates concentrated either close to or far from the grounding line that are expected to drive rapid grounding-line retreat (up to ~ 50 km per century), followed by re-advance when the melt rates are restored to zero.

GMDD
8, 9859–9924, 2015

1.2 Ice Shelf-Ocean Model Intercomparison Projects (ISOMIPs)

ISOMIP was designed in an effort to identify systematic differences between ocean models with sub-shelf cavities. The specifications for the first ISOMIP (Holland et al., 2003; Hunter, 2006) included three idealized experiments with sub-ice-shelf cavities based on Grosfeld et al. (1997). In the first experiment, the entire domain was covered by an ice shelf while the second and third experiments included a sharp calving front and a region of open ocean with smiplified atmospheric/sea ice forcing in the form of surface restoring of temperature and salinity. The restoring was constant in time for the second experiment and varied seasonally in the third. Each experiment was prescribed to run for 30 years, at which point the ocean was expected to be close to steady state.

Unfortunately, ISOMIP results were never collected and compared in a formal publication. The few ISOMIP results that have been published or made publicly available (Hunter, 2015; Losch, 2008; Galton-Fenzi, 2009) suggest that melt rates as well as barotropic and overturning circulations varied between models depending on the vertical discretization and resolution of the model.

In Sect. 3, we describe the design for a second ocean MIP with ice-shelf cavities, ISOMIP+, which aims to improve upon the original ISOMIP in several ways. Bedrock and ice-shelf topographies, based on MISMIP+ results, are more like those of realistic ice shelves in that the water-column thickness goes to zero at the grounding line and the topography varies in 2HD, rather than 1HD. The melt parameterization and parameter choices for horizontal and vertical mixing are closer to those used in realistic applications. The use of far-field restoring, following the approach of Holland et al. (2008) and Goldberg et al. (2012a, b), is more similar to approaches commonly used in forced regional climate experiments. Importantly, preliminary results show that the restoring leads to a quasi-steady state within about a decade, whereas the 30 year ISOMIP experiments approached, but did not reach, a steady state in which the ocean was at the freezing point everywhere. Whereas ISOMIP used static ice-shelf topography, two ISOMIP+ experiments prescribe dynamic topography, allowing models to test

GMDD
8, 9859–9924, 2015

their ability to handle moving boundaries and to see the effects that moving topography has on ocean dynamics.

ISOMIP+ will also improve upon ISOMIP in terms of organised community involvement as well as scientific developments. ISOMIP+ is expected to benefit from the organisation and active community of MISOMIP, as well as the close relationship of ISOMIP+ to both MISMIP+ and MISOMIP1 (through the shared experimental design and development towards coupled ice–ocean models). These factors are likely to lead a larger number of ISOMIP+ participants and formal publication of the analysis, both of which were lacking in ISOMIP.

1.3 Coupled ice sheet-ocean modeling

While no previous MIP has been performed with coupled ice sheet-ocean models, a number of studies have used coupled ice sheet-ocean models, most in idealized configurations. Grosfeld and Sandhäger (2004) performed simulations used offline (file-based) coupling of a 3-D ocean and 2-D ice-sheet model including dynamic calving of tabular icebergs using idealized geometry based on the Filchner-Ronne Ice Shelf. Walker and Holland (2007) and Walker et al. (2008, 2009) used idealized, coupled modeling in 2-D (one horizontal and one vertical dimension) to show that warm ocean conditions and variations in ice basal sliding affected grounding-line motion and ice-shelf topography on decadal timescales. Thoma et al. (2010) coupled 3-D ice-sheet and ocean models to study the dynamics of a sub-glacial lake. Determann et al. (2012) used the same models to perform ice-sheet simulations driven by melt rates computed in the ocean model, showing hysteresis following a melt perturbation applied to idealized ice-sheet geometry. Goldberg et al. (2012a, b) showed results from idealized, coupled experiments spanning 250 years using four different profiles for the ambient water temperature. They showed that feedbacks between the ocean and ice-sheet components led to steepening of the ice draft near the grounding line and strong melting in a channel on the western flank of the ice shelf. Gladish et al. (2012) performed coupled simulations of an idealized ice shelf based on Petermann Glacier with the plume ocean

GMDD
8, 9859–9924, 2015

model in 2HD of Holland and Feltham (2006), showing the influence of channelization on total melt fluxes and melt distribution. Sergienko (2013) used the same plume model to further explore melt channels in idealized configurations. Sergienko et al. (2013) used a plume ocean model in 1HD (Jenkins, 1991) to show that ice-shelf topography is controlled by a balance between ice advection and either ice deformation or ocean melting, depending on the temperature of the ambient ocean water. Walker et al. (2013) used coupled 1-D flowline models to explore the effects of different melt parameterizations on coupled dynamics. While these individual studies have advanced our understanding of ice sheet-ocean processes, a MIP involving coupled ice sheet-ocean models is likely to improve our confidence in the models through greater understanding of the variability and the causes of differences in model results.

In Sect. 4, we describe the first Marine Ice Sheet-Ocean Model Intercomparison Project (MISOMIP1), which combines MISMIP+ and ISOMIP+. In some ways, the MISOMIP1 setup is similar to that of Goldberg et al. (2012a, b) in that it includes a narrow channel with strong ice-shelf buttressing and strong far-field restoring in the ocean. MISOMIP1 differs from this previous work in having (1) steeper channel walls, meaning a stronger change in buttressing as the ice-shelf thickness changes, (2) a larger region of open ocean allowing for ocean dynamics both inside and outside the cavity, and (3) making use of a bedrock topography with an upward-sloping region in the ice-flow direction, allowing us to investigate the possibility that thinning or other changes in the state of the ice sheet could trigger a marine ice-sheet instability (MISI, e.g. Weertman, 1974).

1.4 Goals of the three new MIPs

The MIPs were designed with three main goals in mind. As in their predecessors (ISOMIP, MISMIP and MISMIP3d), the first goal of the MIPs is to provide a controlled forum for researchers to compare their model results with those from other models during model development. Furthermore, it is hoped that researchers will publish their MIP results and/or submit them to the relevant MIP database when they introduce new ice

GMDD
8, 9859–9924, 2015

sheet models, ocean models with ice-shelf cavities or coupled ice sheet-ocean models. Differences between models should be investigated, understood and explained. We have endeavored to keep the MIP setups relatively simple to make them relevant and accessible to the largest possible number of potential contributors and to make them easy to duplicate, while still capturing physical processes relevant to ice sheet-ocean dynamics.

The second goal is that the three MIPs should provide a path for testing components in the process of developing a coupled ice sheet-ocean model. Within ISOMIP+, the experiments progress from static to dynamic (but prescribed) ice geometry with the same goal in mind. Meeting this goal has required that all three MIPs be designed simultaneously, ensuring that they use the same bedrock topography (bathymetry) and compatible domains. Grounding-line dynamics in MISMIP+ are controlled by a melt profile that adapts to the ice geometry and qualitatively mimics example results from ISOMIP+. Ice geometry (both static and dynamic) for ISOMIP+ comes from example results from MISMIP+. In addition, two ISOMIP+ experiments have been designed to produce large changes in melting over a short period of time (less than a decade), mimicking the abrupt changes in melt rate applied in MISMIP+. All three MIPs include an experiment with 100 years of ice retreat followed by 100 years of re-advance, allowing evaluation of standalone and coupled simulations of essentially the same problem.

Our third goal is that each MIP should provide a basic setup from which a large variety of parameter and process studies can usefully be performed. Each MIP setup uses idealized topography and simplifies or ignores known physics. These simplifications leave opportunities for others to study the effects of adding missing processes (e.g. a more realistic calving law, a basal hydrology model, sub-glacial melt water runoff across the grounding line, wind stresses, sea-ice formation and export, tides, time-varying far-field ocean forcing). Results may be affected by parameterizations (e.g. ice sliding law, melt parameterization, mixing schemes in the ocean, equation of state, etc.) and other choices (e.g. horizontal and vertical resolution, coupling interval, ice rheology, etc.) that the community may choose to explore in more detail.

GMDD
8, 9859–9924, 2015

2 MISMIP+ design

The previous Marine Ice Sheet Model Intercomparison Projects, MISMIP and MISMIP3d, tested the capabilities of ice sheet models to simulate advance and retreat cycles under changes in ice softness and basal sliding, respectively, each teaching the community a great deal about the numerical behavior of ice-sheet models of various types. Nonetheless, it was clear in discussions of a follow-up intercomparison exercise that the MISMIP3d experimental design had three shortcomings as a test of 2HD marine ice sheet models. First, it started from a steady state that was invariant in the cross-flow direction – that is, 1HD – and did not involve significant lateral stresses. Second, the initial grounding lines of the shallow-shelf approximation (SSA) (MacAyeal et al., 1996) models were around 80 km downstream from the Stokes models, but the grounding line only moved about 20 km in the perturbation experiment. That left an obvious question entirely unanswered: in a realistic simulation with the model parameters chosen to match geometry and velocity derived from observations, and thus with prescribed initial conditions, does the SSA provide a good approximation to the Stokes model? Third, grounding line migration was driven by changes to the basal traction field, rather than the ice shelf melting that is thought to be the dominant driver of present-day grounding-line retreat in West Antarctica (Joughin et al., 2014; Favier et al., 2014; Seroussi et al., 2014a).

MISMIP+ has been designed to address each of the shortcomings above. Regarding the first, the chosen geometry, based on Gudmundsson et al. (2012), results in strong lateral stresses that buttress the ice stream, and, given particular parameter choices, results in a stable grounding line crossing a retrograde slope, a configuration not possible in 1HD. Regarding the second, modelers are free to choose certain model parameters so that their initial grounding line is close to that of a reference model, and in preliminary tests two models that bracketed the high resolution MISMIP3d results have been found to have grounding lines within a few kilometers of one another in steady state. Finally, extensive grounding line retreat is driven by sub-shelf melt rates.

GMDD
8, 9859–9924, 2015

2.1 Experimental setup

The MISMIP+ domain is a box bounded by $0 \le x \le 640\,\text{km}$ and $0 \le y \le 80\,\text{km}$.[1] The bedrock topography, shown in Fig. 1, is a smaller version of that given in Gudmundsson et al. (2012) and Gudmundsson (2013):

$$B(x,y) = \max\left[B_x(x) + B_y(y), -B_{\max}\right] \tag{1}$$

$$B_x(x) = B_0 + B_2\widetilde{x}^2 + B_4\widetilde{x}^4 + B_6\widetilde{x}^6, \tag{2}$$

$$\widetilde{x} = x/\bar{x} \tag{3}$$

$$B_y(y) = \frac{d_c}{1 + e^{-2(y - L_y/2 - w_c)/f_c}} + \frac{d_c}{1 + e^{2(y - Ly/2 + w_c)/f_c}}, \tag{4}$$

where the parameter values used in these equations, along with several others related to the MISMIP+ experiment, are given in Table 1. As in Gudmundsson et al. (2012), there is a no-slip boundary condition at $x = 0$ and free-slip boundaries at $y = 0$ and 80 km. Ice is removed from the domain beyond $x_{\text{calve}} = 640\,\text{km}$ but no other calving criterion is specified.

Englacial deviatoric stresses τ_{ij} are related to strain-rates D_{ij} through Glen's flow law. As in previous MISMIP exercises,

$$\tau_{ij} = A^{-1/n} D_e^{1/n-1} D_{ij} \tag{5}$$

where $n = 3$. D_e is the second scalar invariant of the strain-rate, given by $2D_e^2 = D_{ij}D_{ji}$, with the usual summation convention. The ice is isothermal, with a constant rate factor A. A suggested value for A is given in Table 1, but participants should modify this value (and/or the coefficient β^2 that appears in the basal traction below) so that the steady state grounding line crosses the center of the trough at $x = 450 \pm 10\,\text{km}$.

[1] The standalone ice sheet experiments place a calving front at $x_{\text{calve}} = 640\,\text{km}$. The same is true of the standalone ocean experiments and the coupled experiments, but the ocean domain extends to $x = 800\,\text{km}$.

GMDD
8, 9859–9924, 2015

The tangential component of the basal traction $\tau_{nt}|_b$ is given by a power law, or by the modified power law relation introduced by Tsai et al. (2015). Participants are free to choose either or both. The power law is

$$\tau_{nt}|_b = \beta^2 |u|^{1/m-1} \boldsymbol{u} \tag{6}$$

where $m = 3$ and a suggested value for the constant β^2 is given in Table 1, but, like A, can be altered so that the steady state grounding line crosses the center of the trough at $x = 450 \pm 10$ km. The modified law differs from the power law by preventing the basal traction from exceeding the value given by a Coulomb law, that is, a fraction of the effective pressure. Assuming the effective pressure at the bed to be approximately hydrostatic:

$$\tau_{nt}|_b = \min\left(\alpha^2 \rho_i g(h - h_f), \beta^2 |u|^{1/m}\right) |u|^{-1} \boldsymbol{u} \tag{7}$$

with $\alpha^2 = 0.5$. h is the ice thickness and

$$h_f = \max\left(0, -\frac{\rho_{sw}}{\rho_i} z_b\right) \tag{8}$$

is the flotation thickness given the bedrock elevation z_b and the reference densities of ice and seawater, ρ_i and ρ_{sw}. Expressing the basal traction in this way ensures that it is continuous (though not differentiable) across the grounding line, but grows to ~ 10–100 kPa over the region ~ 1 km upstream (see Fig 2).

We obtain a formula for computing basal melt by balancing the latent heat of melting with parameterized turbulent heat flux within the ocean (Jenkins et al., 2010), neglecting the heat flux into the ice:

$$m_i = \frac{\rho_i c_w \Gamma_T}{\rho_{fw} L} u_* (T_w - T_f), \tag{9}$$

GMDD
8, 9859–9924, 2015

where ρ_{fw} is the density of fresh water, c_w is the heat capacity of seawater, L is the latent heat of fusion, Γ_T is the heat-transfer coefficient, u_* is the friction velocity and $T_* = (T_w - T_f)$ is the thermal driving, the difference between the ambient ocean water temperature T_w and the local freezing point T_f.

For the purposes of model intercomparison, we have developed an ad-hoc, simplified parameterization of basal melting based on results from Parallel Ocean Program (POP) using cavity shapes from a MISMIP+ simulation. The parameterization prescribes melt rates as follows:

$$m_i = \frac{\rho_i c_w \Gamma_T}{\rho_{fw} L} u_*(H_c) T_*(z_d) \tag{10}$$

$$u_*(H_c) = u_{*,0} \tanh\left(\frac{H_c}{H_{c0}}\right), \tag{11}$$

$$T_*(z_d) = \frac{T_{*,0}}{z_{ref}} |z_d - z_0|, \tag{12}$$

$$H_c = z_d - z_b, \tag{13}$$

where z_d is the elevation of the ice–ocean interface (ice draft), z_b is the elevation of the bedrock topography (bathymetry), H_c is the water-column thickness, and where $u_{*,0}$, $T_{*,0}$ and z_{ref} are fitting constants.

The POP results suggest that the friction velocity u_* increases linearly near the grounding line (for small H_c) but saturates to a nearly constant value when the ocean-cavity thickness exceeds a threshold thickness $H_{c0} = 75$ m. Galton-Fenzi (2009) also showed that melt rates tend to approach zero near the grounding line in a number of experiments, though he found that glacial meltwater fluxes can lead to increased melt rates immediately adjacent to the grounding line. Glacial meltwater fluxes are neglected here. In their idealized simulations studying the behavior of melt water impeded by a bathymetric ridge, De Rydt et al. (2014) saw a similar tapering of the melt rate near the grounding line. It should be noted that melt rates near grounding lines are not well constrained by observations and that ocean models may have particular difficulty

GMDD
8, 9859–9924, 2015

in these regions. Therefore, the dependence upon water column thickness should be treated as an ad-hoc formulation for the purpose of a model intercomparison and not necessarily as a realistic representation of melting near grounding lines.

The POP simulations used to calibrate the parameterization had a temperature profile that increased linearly with depth (similar to the profiles described in Sect. 3.1.3), leading to a thermal driving that also increased approximately linearly with depth. Thermal driving, and therefore melting, reached zero at a depth $z_0 = -100\,\mathrm{m}$. Though the simulations showed some freezing above this depth, we assume for simplicity that no melting or freezing occurs at depths shallower than z_0.

We simplify m_i by lumping various constants and coefficients from Eqs. (10)–(12) into a single coefficient Ω:

$$m_\mathrm{i} = \Omega \tanh\left(\frac{H_\mathrm{c}}{H_{\mathrm{c}0}}\right) \max(z_0 - z_\mathrm{d}, 0)\,. \tag{14}$$

The melt rate as a function of z_d and H_c is shown in Fig 3. Again, the parameter values are given in Table 1. The coefficient Ω has been given a value of $0.2\,\mathrm{yr}^{-1}$, corresponding to a maximum ambient ocean temperature $\sim 1.0\,^\circ\mathrm{C}$, which leads to a melt rate with a maximum value of $m_\mathrm{i} \approx 75\,\mathrm{m\,yr}^{-1}$ near the grounding line (see Fig. 2). We reiterate that the formulation given by Eq. (14) is an ad-hoc parameterization appropriate only for this intercomparison and not appropriate for other geometries, ocean ambient temperatures, etc. The melt parameterization is missing known physics such as dependence on the slope of the ice draft (Goldberg et al., 2012a) and superlinear dependence on ambient ocean temperature (Holland et al., 2008).

2.2 Experiments

MISMIP+ consists of three experiments with different melt rates. Each experiment is initialized by running the model with $m_\mathrm{i} = 0$ (no melting), and should begin with a stable grounding line crossing the center of the channel on the retrograde slope around $x = 450 \pm 10\,\mathrm{km}$. Stable in this case means that the ice sheet thickness and even the

GMDD
8, 9859–9924, 2015

grounding line is permitted to fluctuate, but any fluctuations should average to zero over time, and should be of low amplitude compared to the response to perturbations. Preliminary experiments indicate that, starting from a uniform thickness of 100 m, a stable state is found after around 20,000 yr. One experiment (Ice0) is simply a control, where the melt rate is maintained at $m_i = 0$ for 100 years, while the other two (Ice1 and Ice2) are intended to study the response to substantial ice shelf ablation.

Experiment Ice1 is divided into several parts, all beginning with Ice1r, where the melt rate given in Eq. (14) is applied from $t = 0$ to $t = 100$ yr, and is expected to produce thinning of the ice shelf, a loss of buttressing, and grounding-line retreat. Ice1ra starts from the state computed at the end of the Ice1r simulation and runs at least until $t = 200$ yr, and optionally until $t = 1000$ yr, with no melting, so that the ice shelf thickens, buttressing is restored and the grounding line advances. Preliminary simulations have shown that the grounding-line position does not reach its initial steady state within even 1000 years. Finally, Ice1rr is optional and continues Ice1r, with the melt rate of Eq. (14), until $t = 1000$ yr. Figure 2 shows example basal traction and melt rate fields calculated at several points during the Ice1r and Ice1ra experiments.

Experiment Ice2 is structured in the same way as Ice1, but a different melt rate is applied. The Ice1 melt rate adjusts to pursue the grounding line as it retreats, preventing the formation of a substantive ice shelf. In contrast, Ice2r prescribes a melt-rate of $100\,\mathrm{m\,yr^{-1}}$, where $x > 480$ km and no melt elsewhere from $t = 0$ to $t = 100$ yr, resulting in substantial loss of ice concentrated away from the grounding line, as in a sequence of extensive calving events[2]. Preliminary calculations show that the grounding line retreats for more than 20 km but begins to stabilize as a thick ice shelf forms in its wake. Ice2ra takes the endpoint of the Ice2r experiment as its initial state, and evolves the ice sheet with no melting until $t = 200$ yr and optionally until $t = 1000$ yr, while Ice2rr is optional and continues Ice2r to $t = 1000$ yr.

[2]An alternative would be to have participants move the calving front upstream in Ice2r and allow it to advance in Ice2ra. We chose a melt-rate perturbation instead because it requires the same model capabilities as Ice1.

GMDD
8, 9859–9924, 2015

As an example, Fig. 4 plots grounded area against time for all of the MISMIP+ experiments carried out with the BISICLES ice sheet model using SSA. Table 2 gives a brief summary of the MISMIP+ experiments, as well as those from the other two MIPs.

2.3 Requested output

MISMIP+ requested output is divided into compulsory and optional parts. The compulsory components will be used to write an analysis paper, along the lines of the MISMIP3d paper (Pattyn et al., 2013). The optional data will be included with the compulsory data in an open access database.

Participants are required to supply point data at the grounding line, along the same lines as MISMIP3d, as well as integrated quantities such as volume above flotation, at set times throughout the experiments. Data should be stored in a single NetCDF 4 file for each experiment with the file-naming convention of `[expt]_[MODEL].nc`, where `[expt]` is an experiment name from Table 2 and `[MODEL]` is a unique identifier for the participant. For the core experiments, where $0 \leq t \leq 200$, data should be provided every 10 years starting from $t = 0$, while for the optional extensions, data should be provided every 100 years starting from $t = 200$. Since the length of the grounding line varies over time we expect that the number of point data required to describe it will vary over time in all models.

We ask participants to use the variable and dimension names given in bold and units given in square brackets as follows:

- **nPointGL**. An unlimited dimension – this is a netCDF4 feature that allows **nPointGL** to be decided as the data is written.
- **nTime**. A fixed dimension.
- **time**(nTime) [yr]. The time in years since the beginning of the experiment.

GMDD
8, 9859–9924, 2015

- **iceVolume**(nTime) [m^3], **iceVAF**(nTime) [m^3], **groundedArea**(nTime) [m^2]. The ice volume, volume above flotation, and the grounded area, integrated over the domain.

- **xGL**(nPointGL,nTime), **yGL**(nPointGL,nTime) [m]. The x and y coordinates of a given point on the grounding line.

- **iceThicknessGL**(nPointGL,nTime) [m]. Ice thickness at the grounding line.

- **uBaseGL**(nPointGL,nTime), **vBaseGL**(nPointGL,nTime) [$m\,yr^{-1}$]. The x and y components of the basal velocity.

- **uSurfaceGL**(nPointGL,nTime), **vSurfaceGL**(nPointGL,nTime) [$m\,yr^{-1}$]. The x and y components of the surface velocity.

- **uMeanGL**(nPointGL,nTime), **vMeanGL**(nPointGL,nTime) [$m\,yr^{-1}$]. The x and y components of the vertical mean of the velocity.

Since the number of grounding line points $n(t)$ will vary over time, most of the slices **xGL**(:,t) will contain missing values, which should be filled with the default value `NC_FILL_FLOAT`. In Python, C and Fortran this can be achieved by writing data for each timestep in turn into the first $n(t)$ elements of the slice **xGL**(:,t). At the same time, the unlimited dimension **nPointGL** will be automatically adjusted by the netCDF library routines to the maximum value of $n(t)$. Two python programs are included in the Supplement: write_example.py creates a netcdf file given data in the MISMIP3d text file format, and plot_example.py reads example netcdf files, constructs a plot like Fig. 4, and takes advantage of numpy's masked array class to show the changing shape of the grounding line.

All submissions should include a brief model description, in a. pdf file, which summarizes the stress approximation and parameters used, and evidence that simulations are adequately resolved. The model summary should be an enumerated list, indicating

1. Model: the name of the model (e.g. BISICLES), with a citation if available

GMDD
8, 9859–9924, 2015

2. Englacial stresses: the stress model and coefficients (e.g. SSA, $A = 2.0 \times 10^{-17}\,\mathrm{Pa}^{-3}\,\mathrm{yr}^{-1}$)

3. Basal traction: the choice of law and coefficients, e.g. $|\tau_b| = \beta^2 |u|^{1/3}$, $\beta^2 = 10^4\,\mathrm{Pa\,m}^{-1/3}\,\mathrm{yr}^{1/3}$

4. Space discretization: e.g. finite volume, adaptive non-uniform grid, square cells $0.25\,\mathrm{km} < \Delta x < 4.0\,\mathrm{km}$

5. Time discretization: e.g. Piecewise Parabolic Method, explicit, $\Delta t < \Delta x/(4|u|)$

6. Grounding line: Any special treatment of the grounding line, e.g. one-sided differences of surface elevation

7. MISMIP3d name: The name of the model in MISMIP3d, with any relevant differences, e.g. DMA6 (different mesh resolution)

Evidence that the submissions are adequately resolved will vary from model to model. Conventional models should simply carry out a convergence study of experiment Ice1r and Ice1ra, showing that the grounding line shape and positions at the start and end of Ice1r and the volume-above-flotation curves throughout the experiments converge with mesh refinement and differ by a fraction at the finer resolutions. An example model description is included in the Supplement.

Optionally, participants can add further high-volume data to their NetCDF file. These consist of several fields on a uniform 1 km grid, and are the same fields requested in the coupled IceOcean experiments. They will not be used in the MISMIP+ analysis paper, but will be freely available once the analysis is published. The optional fields are:

- **nx**,**ny**. fixed dimensions, cell-centred points on an 800 × 80 grid of 1 km squares
- **x**(nx) and **y**(ny) [m] cell centers of the output grid as vectors. The grid spacing is 1 km.

GMDD
8, 9859–9924, 2015

- **iceThickness**(nTime,ny,nx) [m] ice thickness.
- **upperSurface**(nTime,ny,nx), **lowerSurface**(nTime,ny,nx) [m] upper and lower surface elevation.
- **basalMassBalance**(nTime,ny,nx) [$\mathrm{m\,yr^{-1}}$] of ice, not water equivalent) basal mass balance (melt rate), positive for melting and negative for freezing.
- **groundedMask**(nTime,ny,nx), **floatingMask**(nTime,ny,nx) the fraction of grounded or floating ice in a given cell.
- **basalTractionMagnitude**(nTime,ny,nx), [Pa] the magnitude of the tangential basal traction field $|\tau_{nt}|_{\mathrm{b}}|$.
- **uBase**(nTime,ny,nx), **vBase**(nTime,ny,nx) [$\mathrm{m\,yr^{-1}}$] x and y components of the basal velocity.
- **uSurface**(nTime,ny,nx), **vSurface**(nTime,ny,nx) [$\mathrm{m\,yr^{-1}}$] x and y components of the surface velocity.
- **uMean**(nTime,ny,nx), **vMean**(nTime,ny,nx) [$\mathrm{m\,yr^{-1}}$] x and y components of the vertical mean of the velocity.

3 ISOMIP+ design

The ISOMIP+ experiments have been designed to make a number of improvements on the original ISOMIP experiments. Whereas ISOMIP used highly idealized geometry (the ocean column at the grounding line was 200 m thick, the ice draft sloped linearly with latitude and was invariant with longitude, and the bedrock was perfectly flat), ISOMIP+ makes use of relatively complex geometry from MISMIP+ BISICLES simulations, including an ocean cavity that reaches zero thickness at the grounding line. Where ISOMIP uses a velocity-independent, two-equation formulation of the melt

GMDD
8, 9859–9924, 2015

boundary conditions, ISOMIP+ uses the velocity-dependent three-equation formulation (e.g. Holland and Jenkins, 1999; Jenkins et al., 2010) more commonly used in realistic model configurations. ISOMIP specified ∼ 10 km resolution, too coarse to resolve the 9 km Rossby radius of deformation (Grosfeld et al., 1997), and large values of the horizontal viscosity and diffusivities, leading to a laminar flow that evolved toward steady state without eddies or other fluctuations. In contrast, ISOMIP+ runs will typically use smaller horizontal viscosity and diffusivities and higher resolution (∼ 2 km), allowing for mesoscale eddies and unsteady flow. A smaller computational domain makes the experiments computationally feasible despite the higher resolution. ISOMIP+ should provide more appropriate test cases than the original ISOMIP for realistic experiments, particularly for those focused on the Amundsen Sea region of WAIS.

ISOMIP+ prescribes four experiments, Ocean1 through Ocean4. Ocean1 and Ocean2 have fixed topography while Ocean3 and Ocean4 have prescribed, evolving ice topography. The experiments are summarized in Table 2.

3.1 Shared setup across the four experiments

We request that ISOMIP+ participants perform each experiment once at a common resolution and with a common set of parameters (hereafter, the COM configuration), and once at a typical resolution and with typical parameters they would use for a realistic problem (hereafter, the TYP configuration). TYP allows participants to choose resolution, parameters and parameterizations typical to each model as it is most often used. We ask participants who do not feel they have time to perform both the COM and TYP experiments to prioritize the COM experiments.

The purpose of COM is to produce results that can be more easily intercompared. We would like to discover the consequences of certain modeling choices (e.g. the horizontal and vertical discretization), in a configuration where as many aspects of the configuration as possible are common to all participating models. TYP will allow us to compare the results of models as they are configured for real problems and to better understand the diversity of results that different modeling choices produce.

GMDD
8, 9859–9924, 2015

Given that there is currently no "right" answer to the ISOMIP+ experiments – there are no observations or exact mathematical solutions with which to compare – the spread in TYP model results are expected to give us insight into how uncertainties reflected in parameter choices affect model solutions.

Parameters general to both COM and TYP runs are given in Table 3, while parameters specific to the COM runs are given in Table 4.

3.1.1 Domain and topography

The ISOMIP+ domain is a Cartesian box bounded by 320 km $\leq x \leq$ 800 km and $0 \leq y \leq 80$ km, overlapping with the right half of the MISMIP+ domain. To aid in describing features within the domain, we define positive x as pointing north (the flow direction of most antarctic ice shelves) and positive y as pointing west. These directions have no dynamic consequences. A region of open ocean extends beyond the edge of the MISMIP+ calving front (which is not allowed to advance beyond $x_{\text{calve}} = 640$ km) on the northern side of the domain. The southern boundary has been placed far enough south to accommodate the retreated ice-shelf geometry used in Ocean2, Ocean3 and Ocean4.

The Coriolis parameter requires latitude to be defined over the domain. We prescribe an f plane configuration at 75° S latitude, although models that do not support an f plane should vary latitude in the x direction with 75° S at the center of the domain (and note this in their `readme` file). Longitude plays no role in the dynamics, and can be defined arbitrarily.

The bathymetry is the same as in Eq. (1). Because the ice-draft geometry is derived from ice-sheet model results, it cannot be described by an analytic function. Instead, both the geometry used for Ocean1 and Ocean2 (see Figs. 5 and 6) and the snapshots used to produce the dynamic geometry for Ocean3 and Ocean4 come from MISMIP+ BISICLES results, and are available in NetCDF format for download from the MISOMIP website (http://www.climate-cryosphere.org/activities/targeted/misomip). The geometry data come from the BISICLES model (Cornford et al., 2013) in the SSA

GMDD
8, 9859–9924, 2015

configuration. The original BISICLES geometry is provided on a 1 km grid so that participants can process the data as they require. We prescribe a slightly coarser resolution, 2 km, for COM runs, since POP simulations indicated that 1 km resolution would be too resource-intensive for the purposes of a MIP. For both COM and TYP runs, participants are expected to interpolate the ice-sheet topography to the ocean grid as part of whatever processing is required to make the data ocean-model friendly (e.g. smoothing; determining regions of land, open ocean and ice-shelf cavity; expanding the water column to a minimum thickness). The calving criterion, described below, should also be applied during this processing step.

3.1.2 Calving

The MISMIP+ experiments explicitly exclude a dynamic calving criterion, allowing the ice to become arbitrarily thin without calving. We felt that it was important that ISOMIP+ include the effects of a cliff-like calving front, so we prescribe a calving criterion on the MISMIP+ geometry used in ISOMIP+. Ocean1 and Ocean2 have stationary geometry, so the calving criterion need only be applied once when setting up the model domain. Ocean3 and Ocean4 have dynamic geometry so it will be necessary to apply calving as the geometry is interpolated in time. Ice thinner than $H_{\text{calve}} = 100$ m (equivalent to an ice draft above ~ -90 m) is considered to have calved and the ice draft is set to zero. To accommodate models that wish to interpolate the MISMIP+ geometry in time for Ocean3 and Ocean4 (see Sect. 3.4 and 3.5), we have not applied the calving criterion to the provided geometry. Calving must be applied as part of setting up the geometry. This prevents the cliff face at the calving front from moving vertically (because of interpolation between large thickness and zero thickness) instead of horizontally in time.

3.1.3 Forcing

There is no forcing at the surface of the open ocean (i.e. no atmospheric or sea-ice fluxes) in any of the experiments. Aside from melt fluxes under the ice shelf, the only

GMDD
8, 9859–9924, 2015

forcing is via 3-D restoring within 10 km of the northern boundary. In the restoring region, potential temperature and salinity are restored to prescribed profiles

$$\frac{\partial T}{\partial t} = \cdots - \gamma(x)\left[T - T_{\mathrm{res}}(z)\right], \tag{15}$$

$$\frac{\partial S}{\partial t} = \cdots - \gamma(x)\left[S - S_{\mathrm{res}}(z)\right], \tag{16}$$

where $T_{\mathrm{res}}(z)$ and $S_{\mathrm{res}}(z)$ are the restoring profiles for potential temperature and salinity, respectively, γ is the decay rate, and where other contributions to the time evolution of T and S have been omitted for simplicity. The decay rate $\gamma(x)$ increases linearly from zero (no restoring) at $x_{\mathrm{r0}} = 790$ km to $\gamma_0 = 10\,\mathrm{days}^{-1}$ at the northern boundary, $x_{\mathrm{r1}} = 800$ km:

$$\gamma(x) = \gamma_0 \max\left(0, \frac{x - x_{\mathrm{r0}}}{x_{\mathrm{r1}} - x_{\mathrm{r0}}}\right). \tag{17}$$

For the initial ocean conditions and boundary forcing, linear depth profiles for potential temperature and salinity are given by

$$T_{\mathrm{res}}(z) = T_0 + (T_{\mathrm{bot}} - T_0)\frac{-z}{B_{\mathrm{max}}}, \tag{18}$$

$$S_{\mathrm{res}}(z) = S_0 + (S_{\mathrm{bot}} - T_0)\frac{-z}{B_{\mathrm{max}}}, \tag{19}$$

where values at the surface (T_0 and S_0) and at the ocean floor (T_{bot} and S_{bot}) vary between the four experiments.

3.1.4 Boundary and initial conditions

In the COM configuration, we request that participants use no-slip lateral boundary conditions at all walls including the northern wall adjacent to the restoring region. We realize that free-slip or open boundary conditions may be more physically justifiable but

GMDD
8, 9859–9924, 2015

no-slip boundary conditions are likely to be supported by the largest number of models. Participants that use other boundary conditions should note this when they submit their results (see Sect. 3.6). The momentum boundary conditions at the ice-shelf base and seabed are quadratic drag with coefficients given in Table 4.

The ocean is initialized at rest with potential temperature and salinity profiles that are horizontally constant. The vertical functional forms of the initial profiles differ between the experiments, and are described below.

For TYP runs, no other model parameters or choices of model physics are prescribed. For COM runs, the recommended values for several relevant parameters are given in Table 4.

3.1.5 COM grid resolution

The nominal horizontal resolution for COM runs is 2 km. We leave it at the discretion of modelers with horizontally unstructured grids to determine what a characteristic resolution of 2 km means for their model.

Given the diversity of ocean-model vertical coordinates, it is not possible or useful to specify a vertical resolution that applies to all models. For this reason, we specify that all models should have 36 vertical layers, but we leave it at the modeler's discretion how the layers are distributed.

Many models will require a minimum ocean-column thickness. We recommend that models make the minimum ocean column as thin as can reasonably be achieved while retaining numerical stability and accuracy. For z level models, the minimum thickness is likely to be approximately two grid cells (~ 40 m if z levels are equally spaced). Models with other vertical coordinates may be less restricted, but "digging" may still be required. We leave it up to each modeler to decide how the "digging" is distributed between the bathymetry and the ice draft. We recommend thickening the ocean column to the minimum thickness wherever the floating mask indicates that ocean is present, as opposed to removing ocean columns that are thinner than a minimum threshold.

GMDD
8, 9859–9924, 2015

We recommend that z level models use both partial top and bottom cells, if they are supported, for increased accuracy.

3.1.6 COM mixing parameterizations

Mixing is typically computed separately in the "horizontal" direction (i.e. within a model layer) and in the "vertical" direction (i.e. between model layers), regardless of which vertical coordinate is being used. To keep the experiments simple, we ask participants to perform "vertical" mixing with the constant vertical viscosities and diffusivities given in Table 4. Most models (e.g. those using the hydrostatic approximation) do not explicitly model convective instability. We prescribe a large vertical viscosity/diffusivity to be applied when the local stratification is unstable, with values given in the table. Participants whose models do not support this convective parameterization should note what other scheme was used to handle unstable stratification (e.g. convective adjustment or explicit modeling of convection).

"Horizontal" mixing should be parameterized with harmonic ("del2") diffusion using a constant eddy viscosity/diffusivity. The values of the "horizontal" eddy viscosity and diffusivity have been chosen so to be small but (hopefully) sufficient to damp grid-scale numerical noise at the COM resolution. Participants may need to increase these values for numerical stability, in which case this should be noted with their results (see Sect. 3.6). The vertical eddy viscosity and diffusivity have the same values as in the original ISOMIP experiment. We note that, in many models, it may be that numerical diffusion is larger than the explicit mixing.

3.1.7 COM equation of state

We prescribe a linear equation of state (EOS) with of coefficients in Table 4:

$$\rho = \rho_{\text{ref}} \left[1 - \alpha_{\text{lin}} (T - T_{\text{ref}}) + \beta_{\text{lin}} (S - S_{\text{ref}})\right]. \quad (20)$$

GMDD
8, 9859–9924, 2015

For models that do not support a linear equation of state, we ask participants to note this and to describe the EOS they used in their `readme` file.

3.1.8 COM melt parameterization

The recommended melt-rate formulation is the three-equation formulation with constant nondimensional heat- and salt-transfer coefficients (Γ_T and Γ_S). Following Jenkins et al. (2010), Eqs. (1), (3), (4) and (5), we have:

$$\rho_{fw} m_w L = -\rho_{sw} c_w u_* \Gamma_T (T_b - T_w), \tag{21}$$

$$T_b = \lambda_1 S_b + \lambda_2 + \lambda_3 p_b, \tag{22}$$

$$\rho_{fw} m_w S_b = -\rho_{sw} u_* \Gamma_S (S_b - S_w), \tag{23}$$

$$u_*^2 = C_{D,top} \left(u_w^2 + u_{tidal}^2 \right), \tag{24}$$

where m_w is the melt rate expressed in water-equivalent (w_{eq}), u_* is the friction velocity, u_w, T_w and S_w are the far-field velocity, potential temperature and salinity in the ocean (see below) and T_b, S_b and p_b are the potential temperature, salinity and pressure at the ice-shelf interface. The prescribed values for the coefficients used in this formulation are given in Table 4.

The liquidous coefficients in Eq. (22) are based on values from Jenkins et al. (2010) but have been modified to compute the potential freezing point. This should save modelers the trouble of converting the boundary-layer potential temperature to in situ temperature before computing the thermal driving. Modelers will need to determine the best method for computing the pressure at the ice–ocean interface, p_b, as we do not prescribe a method for doing so here. One commonly used method (Losch, 2008) computes p_b by integrating a reference density profile from sea level to the ice draft.

For simplicity, the ice is considered to be perfectly insulating. This means that modelers should not use the advection-diffusion scheme from Holland and Jenkins (1999) to determine the heat flux into the ice-shelf, as is common practice in ice-shelf cavity modeling. Top and bottom friction are computed with a quadratic drag law (surface

GMDD
8, 9859–9924, 2015

stresses are proportional to the square of the local ocean flow speed) with drag coefficients, taken from Hunter (2006), given in the table. The root-mean-square "tidal" velocity, u_{tidal}, is used to prevent the friction velocity (and thus the melt rate) from going to zero when there is no motion under the ice shelf. The computation of top and bottom drag do not incorporate u_{tidal}.

Because vertical mixing is a strong function of the distance $z' = |z - z_b|$ from the ice–ocean interface, the heat- and salt-transfer coefficients, Γ_T and Γ_S, are also expected to vary with this distance (McPhee et al., 1987; Jenkins et al., 2010). Sophisticated parameterizations of vertical mixing are presumably required to adequately capture this variability, but such work lies outside the scope of this MIP. Theory suggests that most of the z'-dependence of Γ_S and (to a lesser extent) Γ_T occurs for $z' \lesssim 2\,\text{m}$ (McPhee et al., 1987). However, the theory holds that transfer coefficients are only fully independent of z' when the far-field T and S are sampled outside the turbulent boundary layer. We do not have a broadly accepted theory for how vertical viscosity and diffusivity should vary through the turbulent boundary layer. For simplicity, the COM simulation prescribes constant vertical mixing coefficients (see Sect. 3.1.6), meaning that vertical mixing is not likely to be represented accurately within the boundary layer. Indeed, preliminary results suggest that the melt rates will not converge with vertical resolution in the COM configuration (with constant Γ_T and Γ_S) unless the thickness of the boundary layer is held fixed, independent of the resolution. We prescribe the boundary-layer thickness to be 20 m. Participants should compute the far-field potential temperature, salinity and velocity (T_w, S_w and u_w) either by averaging over the top 20 m (similar to Losch, 2008) or by sampling at a fixed distance $z' = 10\,\text{m}$ below the interface (following the approach of Kimura et al., 2013). The values for Γ_T and Γ_S given in Table 4 were calibrated using the Losch (2008) approach in simulations from the Parallel Ocean Program version 2 extended (POP2x). Transfer coefficients were calibrated so that the maximum melt rate in the first ISOMIP+ experiment (see Sect. 3.2) was $\sim 80\,\text{m}\,\text{yr}^{-1}$, on the order of inferred melt rates near the grounding line of Pine Island Ice Shelf (Dutrieux et al., 2013). Models that are not able to support a boundary-layer of the prescribed

GMDD
8, 9859–9924, 2015

20 m thickness will need to modify the drag coefficient C_D and/or the transfer coefficients Γ_T and Γ_S to arrive at a similar maximum melt rate, in which case this should be noted in the `readme`. The ratio of Γ_T to Γ_S should remain a factor of ~ 35.

Some models will use virtual salt fluxes, while others will use volume fluxes (or perhaps mass fluxes) at the ice–ocean boundary. The freshwater, heat and salt fluxes for models using virtual salt fluxes should be computed following Jenkins et al. (2001) as:

$$F_{\mathrm{fw}} = 0 \tag{25}$$

$$F_H = -c_{\mathrm{w}}\left(\rho_{\mathrm{sw}} u_* \Gamma_T + \rho_{\mathrm{fw}} m_{\mathrm{w}}\right)\left(T_{\mathrm{f}} - T_{\mathrm{w}}\right), \tag{26}$$

$$F_S = -\left(\rho_{\mathrm{sw}} u_* \Gamma_S + \rho_{\mathrm{fw}} m_{\mathrm{w}}\right)\left(S_{\mathrm{b}} - S_{\mathrm{w}}\right). \tag{27}$$

If volume fluxes are used instead, the same fluxes are given by:

$$F_{\mathrm{fw}} = \rho_{\mathrm{fw}} m_{\mathrm{w}} \tag{28}$$

$$F_H = -c_{\mathrm{w}}\left[\rho_{\mathrm{fw}} m_{\mathrm{w}} T_{\mathrm{f}} + \rho_{\mathrm{sw}} u_* \Gamma_T \left(T_{\mathrm{f}} - T_{\mathrm{w}}\right)\right], \tag{29}$$

$$F_S = 0. \tag{30}$$

Though we do not require it, models may wish to use the approach of Losch (2008) in which the melt fluxes are distributed proportionally to all cells in the boundary layer, rather than affecting only the top cell. This approach parameterizes additional vertical mixing within the boundary layer and may prevent noise and/or time-step restrictions in models with very thin cells below the ice–ocean interface.

Models using volume or mass fluxes will need a strategy for removing freshwater in the open ocean to compensate for the volume of melt water that enters the domain. Because of the small size of the domain, without such a strategy, sea level would likely rise by hundreds of meters in simulations with large melt rates (Ocean1 and Ocean3). We recommend imposing an artificial evaporative flux in the open ocean region:

$$F_{\mathrm{e}} = \rho_{\mathrm{sw}} \max\left(\bar{\eta}, 0\right) / \tau_{\mathrm{e}}, \tag{31}$$

GMDD
8, 9859–9924, 2015

where $\tau_e = 30$ days is the characteristic time of the evaporative forcing and η is the mean sea-surface height averaged in space over the open ocean and in time over one month ($\sim \tau_e$) to remove short-term variability. Participants who find that an alternative strategy is more appropriate for their model are asked to document this in the `readme` file supplied with their results.

3.2 ISOMIP+ experiment 1 (Ocean1): cold-to-warm forcing with static ice-shelf geometry

Ocean1 and Ocean2 involve static ice-shelf geometry, making them accessible to a wider range of ocean models. They are intended to represent the most advanced and most retreated states in the coupled ice sheet-ocean system to come later. These experiments are designed to test how changes in far-field ocean forcing result in changes in melt rates, which would drive ice-sheet dynamics in the coupled system. Preliminary simulations with POP2x suggest that, in each experiment, the system will experience an initial shock lasting a few days as the ocean water in contact with the ice shelf adjusts to the melting/freezing boundary conditions. Over several years, changes in ocean properties will propagate from the far field into the ice-shelf cavity, leading to a substantial increase (in Ocean1) or decrease (in Ocean2) in melting.

Ocean1 uses the steady-state geometry shown in Fig. 5, which comes from the initial steady state of the MISMIP+ experiments (see Sect. 2.2) produced with BISICLES using the SSA and no melting. The experiment starts with cold conditions and a low melt rate, consistent with a "cold" Antarctic ice shelf like those bordering the Weddell and Ross Seas. The ocean is initialized with the COLD profiles in Fig. 7, making the deep ocean relatively cold and fresh. Far-field restoring to the WARM profiles (also shown in the figure) leads to warmer and saltier water at depth. The linear profiles of T and S are defined by Eqs. (18) and (19), respectively and parameters for the COLD and WARM profiles are given in Tables 5 and 6, respectively. The WARM profiles was chosen to produce strong thermal driving at depth but potential temperatures near freezing at the surface, qualitatively mimicking observations of deep, warm water observed in the

GMDD
8, 9859–9924, 2015

Amundsen Sea region (Dutrieux et al., 2014). The COLD potential temperature profile is constant at the surface freezing temperature throughout the water column and a lower salinity designed to give a similar density as in the WARM profile throughout the water column (see Fig. 7), thus reducing convective instabilities generated by the restoring. It is worth noting that this COLD-to-WARM scenario represents a transition between the two extremes of water masses observed on the Antarctic continental shelf, and is therefore a highly unrealistic scenario designed purely to test the response of models to an extreme forcing.

The duration of the experiment is exactly 20 years (from the beginning of the date 1 January 0000 to the end of 31 December 0019), which preliminary results suggest is sufficient time to reach a quasi-steady state. Melt rates as well as the strengths of the barotropic and overturning circulations toward the end of the simulation are expected to be significantly larger than those within the first few years because of the warming.

3.3 ISOMIP+ experiment 2 (Ocean2): warm-to-cold forcing with static ice-shelf geometry

In Ocean2, the geometry is from the end of Ice1r (see Sect. 2.2) using BISICLES with the SSA. The geometry is shown in Fig. 6. The ocean is initialized with the WARM profiles and restored to the COLD profiles in Fig. 7, with parameters given in Tables 5 and 6. Again, the experiment should run for 20 years, resulting in a quasi-steady state. As in Ocean1, this is an unrealistic scenario designed purely to evaluate model consistency.

3.4 ISOMIP+ experiment 3 (Ocean3): warm forcing with retreating ice-shelf geometry

Ocean3 begins with the same geometry as Ocean1, but in this experiment the ice draft evolves over time according to a prescribed data set covering 100 years of ice retreat from Ice1r. In this experiment, we prescribe both initialization and restoring to the WARM salinity and potential temperature profile in Fig. 7. Conceptually, this means

GMDD
8, 9859–9924, 2015

we expect strong melting to begin immediately as the sub-ice-shelf circulation spins up, consistent with the strong melt profile prescribed in Ice1r from which the geometry is taken.

On the MISOMIP website, we provide ice geometry at yearly intervals on the original BISICLES 1 km grid. We expect that the frequency with which models can update their geometry may vary considerably, from once per time step in some models to monthly or yearly in others. Modelers wishing to update more frequently than yearly should interpolate the ice draft linearly between subsequent geometries to determine the geometry at intermediate times. As previously mentioned, we have not applied the calving criteria to the geometry provided because calving should be applied only after interpolation in time and space. This means that models that update the geometry only every year and thus require no interpolation in time will need to apply the calving criteria themselves.

3.5 ISOMIP+ experiment 4 (Ocean4): cold forcing with advancing ice-shelf geometry

Conceptually, Ocean4 is an extension of Ocean3. The ice-draft geometry from Ice1ra was produced by abruptly shutting off melting at year 100 and allowing the ice to re-advance for 100 years (see Sect. 2.2). Thus, Ocean4 begins with the final geometry from Ocean3 (which is also the same geometry as in Ocean2). This time, we prescribe both initialization and restoring to the COLD salinity and potential temperature profile, which should lead to very low melt rates, consistent with the lack of melting in the MISMIP+ run that produced the ice geometry. As in Ocean3, yearly topography data at 1 km resolution are provided on the MISOMIP website. Once again, participants will need to apply the calving criteria to these data.

3.6 Requested output

Participants are asked to supply a number of fields interpolated to a standard grid. NetCDF files with example output on the standard grid are supplied on the MISOMIP

GMDD
8, 9859–9924, 2015

website. Participants are asked to supply a single NetCDF4 file for each experiment with the file-naming convention of `[expt]_COM_[MODEL].nc`, where `[expt]` is an experiment name from Table 2, COM or TYP indicates the type of run and `[MODEL]` is a unique identifier for the participant (e.g. the name of the ocean model and/or the institute). We ask participants to provide all fields in 32-bit floating-point precision using the variable and dimension names given in bold and units given in square brackets as follows:

- **nx**, **ny**, **nz** and **nTime** dimensions.
- **x**(nx), **y**(ny) and **z**(nz) [m] cell centers of the output grid as vectors. The origin of the horizontal grid should match MISMIP+ so that the southeast corner of the grid is at $x = 320$ km and $y = 0$. The spacing between horizontal points is 2 km and between vertical points is 5 m.
- **time**(nTime) [s] from the start of the simulation as a vector running over the full duration of the simulation (20 years for Ocean1 and Ocean2, 100 years for Ocean3 and Ocean4). The time interval between entries is one month, using a standard 365 day calendar with no leap years.
- **meanMeltRate**(nTime) [$\mathrm{m\,s^{-1}}$] w_{eq}, the melt rate, positive for melting and negative for freezing, averaged over the ice-shelf base.
- **totalMeltFlux**(nTime) [$\mathrm{kg\,s^{-1}}$], the total mass flux of freshwater across the ice–ocean interface, positive for melting and negative for freezing.
- **totalOceanVolume**(nTime) [$\mathrm{m^3}$], the total volume of the ocean.
- **meanTemperature**(nTime) [°C], the potential temperature averaged over the ocean volume.
- **meanSalinity**(nTime) [PSU], the salinity averaged over the ocean volume.

GMDD
8, 9859–9924, 2015

- **iceDraft**(nTime,ny,nx) [m], the elevation of the ice–ocean interface. Dependence on **time** is only needed for Ocean3 and Ocean4.
- **bathymetry**(nTime,ny,nx) [m], the elevation of the bathymetry. Dependence on **time** is only needed for Ocean3 and Ocean4.
- **meltRate**(nTime,ny,nx) [$\mathrm{m\,s^{-1}}$] w_{eq}, the melt rate, positive for melting and negative for freezing.
- **frictionVelocity**(nTime,ny,nx) [$\mathrm{m\,s^{-1}}$], the friction velocity u_* used in melt calculations.
- **thermalDriving**(nTime,ny,nx) [°C], the thermal driving used in the melt calculation. The thermal driving is the difference between the potential temperature in the boundary layer, T_{w}, and the freezing potential temperature at the ice–ocean interface, T_{b}.
- **halineDriving**(nTime,ny,nx) [PSU], the haline driving used in the melt calculation. The haline driving is the difference between the salinity in the boundary layer, S_{w} and the salinity at the ice–ocean interface, S_{b}.
- **uBoundaryLayer**(nTime,ny,nx) and **vBoundaryLayer**(time, y, x) [$\mathrm{m\,s^{-1}}$], the components of the velocity in the boundary layer that were used to compute u_*.
- **barotropicStreamfunction**(nTime,ny,nx) [$\mathrm{m^3\,s^{-1}}$], the barotropic streamfunction.
- **overturningStreamfunction**(nTime,nz,nx) [$\mathrm{m^3\,s^{-1}}$], the overturning streamfunction in x–z.
- **bottomTemperature**(nTime,ny,nx) [°C] and **bottomSalinity**(nTime,ny,nx) [PSU], the potential temperature and salinity in the bottom-most cell in each ocean column.

GMDD
8, 9859–9924, 2015

– **temperatureXZ**(nTime,nz,nx) [°C] and **salinityXZ**(nTime,nz,nx) [PSU], the potential temperature and salinity slices in x–z plane through the center of the domain, $y = 40$ km.

– **temperatureYZ**(nTime,nz,ny) [°C] and **salinityYZ**(nTime,nz,ny) [PSU], the potential temperature and salinity slices in y–z plane outside the cavity $x = 520$ km.

Invalid values (e.g. field locations that lie within the ice shelf or bedrock) should be masked out using a fill value. In C and Fortran, this can be accomplished by assigning a value of `NC_FILL_FLOAT`. In Python, invalid data can be masked by using numpy masked arrays to assign to netCDF4 variables.

We ask participants to supply monthly mean values of all time-dependent quantities (except **iceDraft** and **bathymetry**, which should be snapshots), where the values in the **time** array indicate the beginning of the period being averaged. Participants who are unable to compute monthly mean values may supply snapshots instead but should indicate this with their submission.

We note that many functions are typically computed on staggered grids. For example, the barotropic streamfunction is typically computed at horizontal cell corners (vertices) and the overturning streamfunction is typically computed at cell corners on the vertical grid. Velocity components (**uBoundaryLayer** and **vBoundaryLayer**) are typically located at cell edges (on a C-grid) or cell corners (on a B-grid). Additionally, for most models, potential temperature and salinity fields will not have values exactly at $y = 40$ km as requested in **temperatureXZ** and **salinityXZ** (and similarly for the y–z slices). To aid in analysis and comparison of results, we ask all participants to interpolate these fields to the standard grid. The standard grid has a high vertical resolution ($\Delta z = 5$ m) in an attempt to accommodate models with a variety of vertical coordinates. Participants are welcome to provide plots of their results on their model's native grid in addition to supplying the output on the standard grid.

GMDD
8, 9859–9924, 2015

Participants are asked to provide the **iceDraft** and **bathymetry**, which are time-dependent for Ocean3 and Ocean4, to show how topography has been modified (interpolated in time, smoothed, the ocean column thickened, etc.).

We ask participants to include a "readme" file (`[expt]_COM_[MODEL].readme`) with their submission describing several specific properties of their model and its ISOMIP+ configuration. These include:

- The name and version of the model used (as specifically as possible, including a citation if available).
- A link to the repository where the model can be downloaded (if public) and specific tag, branch or revision (if available).
- Description of the vertical coordinate of the model (z level, z^*, terrain, isopycnal, etc.).
- Description of how "horizontal" mixing was performed (within model levels, along geopotentials, along isopycnals, etc.).
- Description of the momentum- and tracer-advection schemes used (centered, third-order with limiter, etc.).
- Description of the equation of state.
- Description of the procedure for handling convection (explicitly modeled, parameterized using strong vertical mixing, etc.).
- Description of how T_w, S_w and u_w in the melt parameterization are computed from T, S and $\boldsymbol{u}$ fields (e.g. averaging over the boundary layer, sampling at a fixed distance)
- Description of strategy (if any) for maintaining sea level when volume or mass fluxes are used [e.g. use of Eq. (31)].

GMDD
8, 9859–9924, 2015

- For Ocean3 and Ocean4, a description of how the moving boundary is implemented (e.g. how T, S and $\boldsymbol{u}$ are computed in cells or ocean columns that were previously ice-filled and redistributed, if at all, when a cell or column is filled with ice)
- For TYP results, details on resolution as well as melt and mixing parameterizations.
- For TYP results, a description of the types of problems the participant would typically apply the model to using this configuration (e.g. which region; over what time span; with what kind of initialization, forcing and boundary conditions)
- For COM results, details anywhere the model deviated from the COM resolution or the COM melt and mixing parameterizations.

3.7 Example results

We provide example results as evidence that the experiments are achievable; that Ocean1 and Ocean2 attain the qualitative goals of, respectively, greatly increasing and greatly reducing melting through changes in far-field restoring; and to illustrate the requested output. The example output is not intended to provide a benchmark for other model output.

Example results from Parallel Ocean Program version 2 extended (POP2x) simulations in COM configuration are shown in Figs. 8–12. Figure 8 shows the melt rate averaged over the ice shelf area as a function of time for each experiment. The remaining figures show the requested output fields averaged over the last month of Ocean1 and Ocean3. Animations showing the time-evolution of these fields for all four experiments are available through the MISOMIP website. A version of all four experiments with slightly different parameter values has also been performed successfully with NEMO (the Nucleus for European Modelling of the Ocean).

GMDD
8, 9859–9924, 2015

4 MISOMIP1 design

MISOMIP1 prescribes two coupled ice sheet-ocean experiments (summarized in Table 2), each with two parts. We expect the MISOMIP1 experiment to play an analogous role in evaluating coupled ice sheet-ocean systems to that of the ISOMIP projects for standalone ocean models with ice-shelf cavities and the MISMIP projects for ice-sheet models. We ask participants to first perform the MISMIP+ and ISOMIP+ experiments, so that the behavior of each component on its own has been documented, before proceeding to MISOMIP1.

For both MISOMIP1 experiments, the bedrock topography is the same as for MISMIP+ and ISOMIP+, as given by Eqs. (1)–(4). All ice-sheet parameters are, in general, the same as for MISMIP+ except where noted below. To simplify the coupled problem, we prescribe a constant ice temperature as in MISMIP+ and set the thermal conductivity of ice to zero (so that there is no sensible heat flux into ice at the ice–ocean interface). Thus, the only flux across the ice–ocean interface is of melt water.

4.1 MISOMIP1 experiment 1 (IceOcean1): retreat and re-advance without dynamic calving

IceOcean1 begins with the ice-sheet steady state that also served as the initial conditions for the Ice0, Ice1 and Ice2 experiments (see Sect. 2.2). Unlike in ISOMIP+, IceOcean1 does not include a dynamic calving criterion. Ice is allowed to become as thin as the ice sheet and ocean components permit (potentially zero thickness) without calving.

The experiment consists of two phases – a 100 year retreat phase, IceOcean1r, and a 100 year re-advance phase, IceOcean1ra. At the beginning of IceOcean1r, the ocean component is initialized with the steady-state ice topography and the COLD salinity and temperature profiles from Fig. 7 and Table 5. The initial state should be cold enough to produce low melt rates ($\sim 0.2\,\mathrm{m\,yr^{-1}}$ in preliminary tests) that are approximately consistent with the ice sheet's initial state. For the 100 year duration of IceOcean1r, restor-

GMDD
8, 9859–9924, 2015

ing to the WARM profile (see Fig. 7 and Table 6) is applied near the ocean's northern boundary. As in Ocean1, the warm water is expected to reach the ice-shelf cavity within the first decade, at which point it should induce strong melting and subsequent rapid ice retreat.

The re-advance phase, IceOcean1ra, begins where IceOcean1r ends but abruptly switches to the COLD restoring profile at the ocean's northern boundary. This should greatly reduce melting within a decade, similarly to Ocean2, and allow ice to re-advance for the remaining 100 years of simulation.

4.2 MISOMIP1 experiment 2 (IceOcean2; optional): retreat and re-advance with dynamic calving

Specifying calving is a major problem in the design of MISOMIP1. There was general agreement in the community that ice-sheet models have not been shown to behave reliably with dynamic calving, nor is there any consensus about which calving parameterizations are appropriate or physically realistic. In Antarctica, calving events tend to be infrequent, producing large tabular icebergs, a process that is not well modeled by a continuous calving velocity or a simple calving criterion such as that used on ISOMIP+ (see Sect. 3.1.2). Nevertheless, we felt that it was important for testing the robustness of the ice-sheet and ocean components in MISOMIP1 that there be an experiment with a dynamic, sheer cliff at the calving front. We include an optional coupled experiment, IceOcean2, that is identical to IceOcean1 except that it includes dynamic calving in the ice-sheet component.

Whereas the MISMIP+ experiments do not include a dynamic calving front, IceOcean2 prescribes the same simple calving criterion used in ISOMIP+: ice thinner than $H_{\text{calve}} = 100\,\text{m}$ (equivalent to an ice draft above $\sim -90\,\text{m}$) or beyond $x_{\text{calve}} = 640\,\text{km}$ should be calved and the ice thickness set to zero. The calving criterion should be enforced in the ice-sheet component.

Because the calving criterion will change the steady state of the ice sheet, IceOcean2 should begin with a new ice-sheet spinup, again without melting but with the

GMDD
8, 9859–9924, 2015

calving criterion imposed. As in MISMIP+, participants should modify the ice softness (A) and/or the basal-traction coefficient (β^2) so that the steady state grounding line crosses the center of the trough at $x = 450 \pm 10$ km. Participants may wish to perform the Ice1 experiment with the calving criterion, but this is not required.

4.3 Component resolutions and parameterizations

As in the ISOMIP+ experiments, we ask participants to perform the MISOMIP1 experiment once in a "common" (COM) configuration similar to that of ISOMIP+. For this configuration, the ocean component should have the same resolution and parameters as in the ISOMIP+ COM run. We do not prescribe the resolution of the ice-sheet component because the wider use of unstructured, dynamic and adaptive grids as well as higher-order elements in ice-sheet models compared with ocean models make it impractical to provide specifications that are appropriate for all models. Also, grounding-line dynamics in ice sheet models have been shown to converge with resolution (e.g. Durand et al., 2009; Cornford et al., 2013; Leguy et al., 2014), whereas the same has not been shown for melt rates in ocean models. Since different ice stress approximations produce different results even at very high resolution (Pattyn et al., 2012, 2013), the evaluation will likely be most effective when comparing ice components using the same stress approximation. For this reason, we request that participants submit COM results using the shallow shelf approximation (SSA) if possible. COM results with other stress approximations are also welcome.

Whereas we prescribed a "typical" run for ISOMIP+ with resolution and parameters that the ocean model typically uses for Antarctic regional simulations, it is not obvious that this is appropriate for MISOMIP1 models. Coupled ice sheet-ocean models are not well enough established to have typical resolutions and parameters. Therefore, we invite participants to submit several sets of results with parameter choices at their discretion in addition to the COM run and ensure these are well documented in the `readme` file.

GMDD
8, 9859–9924, 2015

The coupling interval for the model is left to each participant to decide. We recommend based on experience with the POPSICLES (coupled POP2x and BISICLES) model that participants use a coupling interval of six months or less if they are able, as results with yearly coupling diverged significantly from those with more frequent coupling. We ask participants who are able to do so to provide multiple sets of results using different coupling intervals.

4.4 Requested output

We request that participants supply separate NetCDF files for their ice-sheet and ocean MISOMIP1 results. This allows the results to be supplied on different grids and is expected to simplify comparing the final results. NetCDF files with example output on the standard grids for each component are supplied on the MISOMIP website (http://www.climate-cryosphere.org/activities/targeted/misomip). Participants are asked to supply all fields in 32-bit floating-point precision, with the file-naming convention of `[expt]_COM_[component]_[MODEL_CONFIG].nc`, where `[expt]` is the experiment name from Table 2, COM indicates a verification run and is omitted for non-COM runs, `[component]` is either ice or ocean and `[MODEL_CONFIG]` is a unique identifier for the coupled-model configuration (e.g. the name of the model, the institute, ice stress approximation, etc.).

The requested ocean fields and the output grid are the same as in Sect. 3.6. The requested output from the ice-sheet component is the same as in MISMIP+ (see Sect. 2.3) with the exception that `time` is sampled monthly, the 2-D fields are required, rather than optional, and time should be given in s rather than yr for consistency with the ocean output. As in MISMIP+, the 2-D ice-sheet fields should be interpolated from the ice-sheet model's native grid to the standard 1 km grid to simplify analysis.

GMDD
8, 9859–9924, 2015

4.5 Example results

Example results from POPSICLES (POP2x-BISICLES) simulations are shown in Fig. 13. An animated version of the first panel is available on the MISOMIP website. The figure shows the ice geometry as well as the basal melt rate and the ocean temperature at the end of POPSICLES IceOcean1r simulation. The ice draft has steepened near the grounding line where the majority of melting now occurs. The figure also shows the grounded ice area and mean melt rate as functions of time over IceOcean1. At present, we have not completed a simulation of the IceOcean2 experiment, but example results produced with POPSICLES will be made available on the MISOMIP website as soon as they are completed.

5 Conclusions

Here, we have described the experimental design for three interrelated model intercomparison projects (MIPs): the third Marine Ice Sheet MIP (MISMIP+), the second Ice Shelf-Ocean MIP (ISOMIP+) and the first Marine Ice Sheet-Ocean MIP (MISOMIP1). We expect that the results from each MIP will be published separately with all contributors as coauthors, following the tradition of the earlier MISMIPs.

We have demonstrated that all experiments are achievable with typical ice and ocean models (BISICLES, POP2x and POPSICLES), and that the results are consistent with the intended behavior behind the experimental design. The MISMIP+ experiments show significant grounding-line dynamics in response to forcing by basal melting (Ice1) and a large calving event (Ice2). Two ISOMIP+ experiments, Ocean1 and Ocean2, demonstrate that changes in far-field forcing can lead to basal melting being significantly enhanced or suppressed on decadal timescales. The remaining ISOMIP+ experiments, Ocean3 and Ocean4, provide a meaningful test of whether ocean models can handle dynamic ice-shelf geometry. The main MISOMIP1 experiment, IceOcean1, demonstrates that changes in far-field ocean conditions can induce significant

GMDD
8, 9859–9924, 2015

grounding-line dynamics. An optional experiment, IceOcean2, demonstrates that both the ice-sheet and ocean components can handle a dynamic calving front.

The Supplement related to this article is available online at doi:10.5194/gmdd-8-9859-2015-supplement.

Acknowledgements. This material is based upon work supported by the U.S. Department of Energy, Office of Science, Office of Biological and Environmental Research under Award Numbers DE-SC0011982 and DE-SC0013038. Support was provided through NYU Abu Dhabi grant G1204. Simulation results were produced using resources of the National Energy Research Scientific Computing Center, a DOE Office of Science User Facility supported by the Office of Science of the U.S. Department of Energy under Contract No. DE-AC02-05CH11231. This work has received funding from the European Union Seventh Framework Programme (FP7/2007-2013) under grant agreement number 299035. Work at the Lawrence Berkeley National Laboratory was supported by the Director, Office of Science, Office of Advanced Scientific Computing Research, of the U.S. Department of Energy under Contract No. DE-AC02-05CH11231.

References

Cornford, S. L., Martin, D. F., Graves, D. T., Ranken, D. F., Le Brocq, A. M., Gladstone, R. M., Payne, A. J., Ng, E. G., and Lipscomb, W. H.: Adaptive mesh, finite volume modeling of marine ice sheets, J. Comput. Phys., 232, 529–549, doi:10.1016/j.jcp.2012.08.037, 2013. 9863, 9879, 9897

De Rydt, J., Holland, P. R., Dutrieux, P., and Jenkins, A.: Geometric and oceanographic controls on melting beneath Pine Island Glacier, J. Geophys. Res.-Oceans, 119, 2420–2438, doi:10.1002/2013JC009513, 2014. 9871

Determann, J., Thoma, M., Grosfeld, K., and Massmann, S.: Impact of ice-shelf basal melting on inland ice-sheet thickness: a model study, Ann. Glaciol., 53, 129–135, doi:10.3189/2012AoG60A170, 2012. 9865

GMDD
8, 9859–9924, 2015

Drouet, A. S., Docquier, D., Durand, G., Hindmarsh, R., Pattyn, F., Gagliardini, O., and Zwinger, T.: Grounding line transient response in marine ice sheet models, The Cryosphere, 7, 395–406, doi:10.5194/tc-7-395-2013, 2013. 9863

Durand, G., Gagliardini, O., de Fleurian, B., Zwinger, T., and Le Meur, E.: Marine ice sheet dynamics: hysteresis and neutral equilibrium, J. Geophys. Res., 114, F03009, doi:10.1029/2008JF001170, 2009. 9863, 9897

Dutrieux, P., Vaughan, D. G., Corr, H. F. J., Jenkins, A., Holland, P. R., Joughin, I., and Fleming, A. H.: Pine Island glacier ice shelf melt distributed at kilometre scales, The Cryosphere, 7, 1543–1555, doi:10.5194/tc-7-1543-2013, 2013. 9885

Dutrieux, P., De Rydt, J., Jenkins, A., Holland, P. R., Ha, H. K., Lee, S. H., Steig, E. J., Ding, Q., Abrahamsen, E. P., and Schroder, M.: Strong sensitivity of pine island ice-shelf melting to climatic variability, Science, 3, 468–472, doi:10.1126/science.1244341, 2014. 9888, 9918

Favier, L., Durand, G., Cornford, S. L., Gudmundsson, G. H., Gagliardini, O., Gillet-Chaulet, F., Zwinger, T., Payne, A. J., and Le Brocq, A. M.: Retreat of Pine Island Glacier controlled by marine ice-sheet instability, Nature Clim. Change, 5, 1–5, doi:10.1038/nclimate2094, 2014. 9868

Feldmann, J. and Levermann, A.: Interaction of marine ice-sheet instabilities in two drainage basins: simple scaling of geometry and transition time, The Cryosphere, 9, 631–645, doi:10.5194/tc-9-631-2015, 2015. 9863

Feldmann, J., Albrecht, T., Khroulev, C., Pattyn, F., and Levermann, A.: Resolution-dependent performance of grounding line motion in a shallow model compared with a full-Stokes model according to the MISMIP3d intercomparison, J. Glaciol., 60, 353–360, doi:10.3189/2014JoG13J093, 2014. 9863

Galton-Fenzi, B. K.: Modeling Ice-shelf/Ocean Interactions, PhD thesis, University of Tasmania, Hobart, Tasmania, Australia, 2009. 9864, 9871

Gladish, C. V., Holland, D. M., Holland, P. R., and Price, S. F.: Ice-shelf basal channels in a coupled ice/ocean model, J. Glaciol., 58, 1527–1544, doi:10.3189/2012JoG12J003, 2012. 9865

Gladstone, R. M., Payne, A. J., and Cornford, S. L.: Parameterising the grounding line in flowline ice sheet models, The Cryosphere, 4, 605–619, doi:10.5194/tc-4-605-2010, 2010. 9863

Goldberg, D. N., Little, C. M., Sergienko, O. V., Gnanadesikan, A., Hallberg, R., and Oppenheimer, M.: Investigation of land ice–ocean interaction with a fully coupled ice–

GMDD
8, 9859–9924, 2015

ocean model: 1. Model description and behavior, J. Geophys. Res., 117, F02037, doi:10.1029/2011JF002246, 2012a. 9864, 9865, 9866, 9872
Goldberg, D. N., Little, C. M., Sergienko, O. V., Gnanadesikan, A., Hallberg, R., and Oppenheimer, M.: Investigation of land ice–ocean interaction with a fully coupled ice–ocean model: 2. Sensitivity to external forcings, J. Geophys. Res., 117, F02038, doi:10.1029/2011JF002247, 2012b. 9864, 9865, 9866
Grosfeld, K. and Sandhäger, H.: The evolution of a coupled ice shelf–ocean system under different climate states, Global Planet. Change, 42, 107–132, doi:10.1016/j.gloplacha.2003.11.004, 2004. 9865
Grosfeld, K., Gerdes, R., and Determann, J.: Thermohaline circulation and interaction between ice shelf cavities and the adjacent open ocean, J. Geophys. Res., 102, 15595–15610, doi:10.1029/97JC00891, 1997. 9864, 9878
Gudmundsson, G. H.: Ice-shelf buttressing and the stability of marine ice sheets, The Cryosphere, 7, 647–655, doi:10.5194/tc-7-647-2013, 2013. 9863, 9869
Gudmundsson, G. H., Krug, J., Durand, G., Favier, L., and Gagliardini, O.: The stability of grounding lines on retrograde slopes, The Cryosphere, 6, 1497–1505, doi:10.5194/tc-6-1497-2012, 2012. 9863, 9868, 9869
Holland, D. M. and Jenkins, A.: Modeling thermodynamic ice–ocean interactions at the base of an ice shelf, J. Phys. Oceanogr., 29, 1787–1800, doi:10.1175/1520-0485(1999)029<1787:MTIOIA>2.0.CO;2, 1999. 9878, 9884
Holland, D. M., Hunter, J., Grosfeld, K., Hellmer, H., Jenkins, A., Morales Maqueda, M. A., Hemer, M., Williams, M., Klinck, J. M., and Dinniman, M.: The Ice Shelf – Ocean Model Intercomparison Project (ISOMIP), Eos Trans. AGU, 84(46), Fall Meet. Suppl., Abstract C41A–05, 2003. 9864
Holland, P. R. and Feltham, D. L.: The effects of rotation and ice shelf topography on Frazil-Laden ice shelf water plumes, J. Phys. Oceanogr., 36, 2312–2327, doi:10.1175/JPO2970.1, 2006. 9866
Holland, P. R., Jenkins, A., and Holland, D. M.: The response of ice shelf basal melting to variations in ocean temperature, J. Climate, 21, 2558–2572, doi:10.1175/2007JCLI1909.1, 2008. 9864, 9872
Hunter, J. R.: Specification for test models of ice shelf cavities, Tech. Rep. June, Antarctic Climate and Ecosystems Cooperative Research Centre, available at: http://staff.acecrc.org.au/~johunter/isomip/test_cavities.pdf (last access: 7 November 2015), 2006. 9864, 9885

GMDD
8, 9859–9924, 2015

Hunter, J. R.: ISOMIP Files, available at: http://staff.acecrc.org.au/~johunter/isomip/isomip.html, last access: 30 June 2015. 9864
Jenkins, A.: A one-dimensional model of ice shelf-ocean interaction, J. Geophys. Res., 96, 20671–20677, doi:10.1029/91JC01842, 1991. 9866
Jenkins, A., Hellmer, H. H., and Holland, D. M.: The role of meltwater advection in the formulation of conservative boundary conditions at an ice–ocean interface, J. Phys. Oceanogr., 31, 285–296, doi:10.1175/1520-0485(2001)031<0285:TROMAI>2.0.CO;2, 2001. 9886
Jenkins, A., Nicholls, K. W., and Corr, H. F. J.: Observation and parameterization of ablation at the base of Ronne Ice Shelf, Antarctica, J. Phys. Oceanogr., 40, 2298–2312, doi:10.1175/2010JPO4317.1, 2010. 9870, 9878, 9884, 9885
Joughin, I., Smith, B. E., and Medley, B.: Marine ice sheet collapse potentially under way for the Thwaites Glacier Basin, West Antarctica, Science, 344, 735–738, doi:10.1126/science.1249055, 2014. 9868
Kimura, S., Candy, A., Holland, P., Piggott, M., and Jenkins, A.: Adaptation of an unstructured-mesh, finite-element ocean model to the simulation of ocean circulation beneath ice shelves, Ocean Model., 67, 39–51, doi:10.1016/j.ocemod.2013.03.004, 2013. 9885
Leguy, G. R., Asay-Davis, X. S., and Lipscomb, W. H.: Parameterization of basal friction near grounding lines in a one-dimensional ice sheet model, The Cryosphere, 8, 1239–1259, doi:10.5194/tc-8-1239-2014, 2014. 9863, 9897
Losch, M.: Modeling ice shelf cavities in a z coordinate ocean general circulation model, J. Geophys. Res., 113, 1–15, doi:10.1029/2007JC004368, 2008. 9864, 9884, 9885, 9886
MacAyeal, D., Rommelaere, V., Huybrechts, P., Hulbe, C., Determann, J., and Ritz, C.: An ice-shelf model test based on the Ross ice shelf, Ann. Glaciol., 23, 46–51, 1996. 9868
McPhee, M. G., Maykut, G. A., and Morison, J. H.: Dynamics and thermodynamics of the ice/upper ocean system in the marginal ice zone of the Greenland Sea, J. Geophys. Res., 92, 7017–7031, doi:10.1029/JC092iC07p07017, 1987. 9885
Pattyn, F., Schoof, C., Perichon, L., Hindmarsh, R. C. A., Bueler, E., de Fleurian, B., Durand, G., Gagliardini, O., Gladstone, R., Goldberg, D., Gudmundsson, G. H., Huybrechts, P., Lee, V., Nick, F. M., Payne, A. J., Pollard, D., Rybak, O., Saito, F., and Vieli, A.: Results of the Marine Ice Sheet Model Intercomparison Project, MISMIP, The Cryosphere, 6, 573–588, doi:10.5194/tc-6-573-2012, 2012. 9862, 9897
Pattyn, F., Perichon, L., Durand, G., Favier, L., Gagliardini, O., Hindmarsh, R. C. A., Zwinger, T., Albrecht, T., Cornford, S., Docquier, D., Fürst, J. J., Goldberg, D., Gudmunds-

GMDD
8, 9859–9924, 2015

son, G. H., Humbert, A., Hütten, M., Huybrechts, P., Jouvet, G., Kleiner, T., Larour, E., Martin, D., Morlighem, M., Payne, A. J., Pollard, D., Rückamp, M., Rybak, O., Seroussi, H., Thoma, M., and Wilkens, N.: Grounding-line migration in plan-view marine ice-sheet models: results of the ice2sea MISMIP3d intercomparison, J. Glaciol., 59, 410–422, doi:10.3189/2013JoG12J129, 2013. 9863, 9874, 9897

Schoof, C.: Marine ice-sheet dynamics. Part 1. The case of rapid sliding, J. Fluid Mech., 573, 27, doi:10.1017/S0022112006003570, 2007a. 9862

Schoof, C.: Ice sheet grounding line dynamics: steady states, stability, and hysteresis, J. Geophys. Res., 112, 1–19, doi:10.1029/2006JF000664, 2007b. 9862

Sergienko, O. V.: Basal channels on ice shelves, J. Geophys. Res.-Earth, 118, 1342–1355, doi:10.1002/jgrf.20105, 2013. 9866

Sergienko, O. V., Goldberg, D. N., and Little, C. M.: Alternative ice shelf equilibria determined by ocean environment, J. Geophys. Res.-Earth, 118, 970–981, doi:10.1002/jgrf.20054, 2013. 9866

Seroussi, H., Morlighem, M., Larour, E., Rignot, E., and Khazendar, A.: Hydrostatic grounding line parameterization in ice sheet models, The Cryosphere, 8, 2075–2087, doi:10.5194/tc-8-2075-2014, 2014a. 9868

Seroussi, H., Morlighem, M., Rignot, E., Mouginot, J., Larour, E., Schodlok, M., and Khazendar, A.: Sensitivity of the dynamics of Pine Island Glacier, West Antarctica, to climate forcing for the next 50 years, The Cryosphere, 8, 1699–1710, doi:10.5194/tc-8-1699-2014, 2014b. 9863

Thoma, M., Grosfeld, K., Mayer, C., and Pattyn, F.: Interaction between ice sheet dynamics and subglacial lake circulation: a coupled modelling approach, The Cryosphere, 4, 1–12, doi:10.5194/tc-4-1-2010, 2010. 9865

Tsai, V. C., Stewart, A. L., and Thompson, A. F.: Marine ice-sheet profiles and stability under Coulomb basal conditions, J. Glaciol., 61, 205–215, doi:10.3189/2015JoG14J221, 2015. 9863, 9870, 9913, 9915

Walker, R. T. and Holland, D. M.: A two-dimensional coupled model for ice shelf–ocean interaction, Ocean Model., 17, 123–139, doi:10.1016/j.ocemod.2007.01.001, 2007. 9865

Walker, R. T., Dupont, T. K., Parizek, B. R., and Alley, R. B.: Effects of basal-melting distribution on the retreat of ice-shelf grounding lines, Geophys. Res. Lett., 35, L17503, doi:10.1029/2008GL034947, 2008. 9865

GMDD
8, 9859–9924, 2015

Walker, R. T., Dupont, T. K., Holland, D. M., Parizek, B. R., and Alley, R. B.: Initial effects of oceanic warming on a coupled ocean–ice shelf–ice stream system, Earth Planet. Sc. Lett., 287, 483–487, doi:10.1016/j.epsl.2009.08.032, 2009. 9865

Walker, R. T., Holland, D. M., Parizek, B. R., Alley, R. B., Nowicki, S. M. J., and Jenkins, A.: Efficient flowline simulations of ice-shelf/ocean interactions: sensitivity studies with a fully coupled model, J. Phys. Oceanogr., 43, 2200–2210, doi:10.1175/JPO-D-13-037.1, 2013. 9866

Weertman, J.: Stability of the junction of an ice sheet and an ice shelf, J. Glaciol., 13, 3–11, 1974. 9866

GMDD

8, 9859–9924, 2015

Table 1. Parameters for the MISMIP+ experiments.

Parameter	Value	Description
L_x	640 km	Domain length (along ice flow)
L_y	80 km	Domain width (across ice flow)
B_0	−150.0 m	Bedrock topography at $x = 0$
B_2	−728.8 m	Second bedrock topography coefficient
B_4	343.91 m	Third bedrock topography coefficient
B_6	−50.57 m	Fourth bedrock topography coefficient
$\bar{x}$	300 km	Characteristic along-flow length scale of the bedrock
f_c	4.0 km	Characteristic width of the side walls of the channel
d_c	500 m	Depth of the trough compared with the side walls
w_c	24.0 km	Half-width of the trough
B_{max}	720 m	Maximum depth of the bedrock topography
x_{calve}	640 km	The location in x beyond which ice is removed
ρ_i	918 kg m^{-3}	Density of ice
ρ_{sw}	1028 kg m^{-3}	Density of seawater
Ω	−0.2 yr^{-1}	Melt-rate rate factor
z_0	−100 m	Depth above which the melt rate is zero
H_{c0}	75 m	Reference ocean cavity thickness
a	0.3 m yr^{-1}	Accumulation rate
A	6.338×10^{-25} Pa^{-3} s^{-1} $= 2.0 \times 10^{-17}$ Pa^{-3} yr^{-1}	Glen's law coefficient
n	3	Glen's law exponent
m	3	Friction-law exponent
α^2	0.5	Coulomb law friction coefficient
β^2	3.160×10^6 Pa m$^{-1/3}$ s$^{1/3}$ $= 1.0 \times 10^4$ Pa m$^{-1/3}$ yr$^{1/3}$	Power law friction coefficient
–	31 556 926 s yr^{-1}	Seconds per year (defined to have 365.2422 days)

GMDD
8, 9859–9924, 2015

Table 2. A list of the MISMIP+, ISOMIP+ and MISOMIP1 experiments.

MIP	Experiment	Description
MISMIP+	Ice0	100 year control simulation with no melting
MISMIP+	Ice1r	100 year run with melt-induced retreat
MISMIP+	Ice1ra	100 year (or optionally up to 900 year) simulation from end of Ice1r with no melting
MISMIP+	Ice1rr	Continue Ice1r for a further 900 years (optional)
MISMIP+	Ice2r	100 year "calving event" simulation
MISMIP+	Ice2ra	100 year (or optionally up to 900 year) simulation from end of Ice2r with no melting
MISMIP+	Ice2rr	Continue Ice2r for a further 900 years (optional)
ISOMIP+	Ocean1	20 year run with static geometry, COLD initial conditions and WARM forcing
ISOMIP+	Ocean2	20 year run with static geometry, WARM initial conditions and COLD forcing
ISOMIP+	Ocean3	100 year run with dynamic geometry, WARM initial conditions and WARM forcing
ISOMIP+	Ocean4	100 year run with dynamic geometry, COLD initial conditions and COLD forcing
MISOMIP1	IceOcean1r	100 year coupled run with no dynamic calving, COLD initial conditions and WARM forcing
MISOMIP1	IceOcean1ra	100 year coupled run from end of IceOcean1r with no dynamic calving and COLD forcing
MISOMIP1	IceOcean2r	Optional: 100 year coupled run with dynamic calving, COLD initial conditions and WARM forcing
MISOMIP1	IceOcean2ra	Optional: 100 year coupled run from end of IceOcean2r with dynamic calving and COLD forcing

GMDD
8, 9859–9924, 2015

Table 3. Parameters shared between all four ISOMIP+ experiments.

Parameter	Value	Description
L_x	480 km	Domain length (along ice flow)
L_y	80 km	Domain width (across ice flow)
H_{calve}	100 m	The minimum thickness of ice, below which it is removed
θ_c	75° S	Latitude of the center of the domain
γ_0	10 days^{-1}	The restoring decay rate at the northern boundary
x_{r0}	790 km	The southern edge of the restoring region
x_{r1}	800 km	The northern edge of the restoring region

GMDD
8, 9859–9924, 2015

Table 4. Parameters recommended for the common (COM) experiments.

Parameter	Value	Description
$\Delta x = \Delta y$	2 km	Horizontal resolution
c_w	3974 J °C^{-1} kg^{-1}	Specific heat capacity of seawater
L	3.34×10^5 J kg^{-1}	Latent heat of fusion of ice
λ_1	−0.0573 °C PSU^{-1}	Liquidus slope
λ_2	0.0832 °C	Liquidus intercept
λ_3	-7.53×10^{-8} °C Pa^{-1}	Liquidus pressure coefficient
Γ_T	5.0×10^{-2}	Nondimensional heat-transfer coefficient
Γ_S	1.4×10^{-3}	Nondimensional salt-transfer coefficient
$C_{D,top}$	2.5×10^{-3}	Top drag coefficient
$C_{D,bot}$	2.5×10^{-3}	Bottom drag coefficient
u_{tidal}	0.01 m s^{-1}	RMS velocity associated with tides
κ_i	0	Heat diffusivity into ice (perfectly insulating)
ν_{unstab}	0.1 m^2 s^{-1}	Convective vertical viscosity
κ_{unstab}	0.1 m^2 s^{-1}	Convective vertical diffusivity
ν_{stab}	1×10^{-3} m^2 s^{-1}	Stable vertical eddy viscosity
κ_{stab}	5×10^{-5} m^2 s^{-1}	Stable vertical eddy diffusivity
ν_H	6.0 m^2 s^{-1}	Horizontal eddy viscosity
κ_H	1.0 m^2 s^{-1}	Horizontal eddy diffusivity
ρ_{fw}	1000 kg m^{-3}	Density of fresh water
ρ_{sw}	1028 kg m^{-3}	Reference density of seawater
T_{ref}	−1 °C	reference potential temperature for linear EOS
S_{ref}	34.2 PSU	reference salinity for linear EOS
ρ_{ref}	1027.51 kg m^{-3}	in-situ density for linear EOS
α_{lin}	3.733×10^{-5} °C^{-1}	thermal expansion coefficient for linear EOS
β_{lin}	7.843×10^{-4} PSU^{-1}	salinity contraction coefficient for linear EOS

GMDD
8, 9859–9924, 2015

Table 5. Parameters for the COLD profiles.

Parameter	Value	Description
T_0	−1.9 °C	Surface temperature
T_{bot}	−1.9 °C	Temperature at the ocean floor
S_0	33.8 PSU	Surface salinity
S_{bot}	34.55 PSU	Salinity at the ocean floor

GMDD
8, 9859–9924, 2015

Table 6. Parameters for the WARM profiles.

Parameter	Value	Description
T_0	−1.9 °C	Surface temperature
T_{bot}	1.0 °C	Temperature at the ocean floor
S_0	33.8 PSU	Surface salinity
S_{bot}	34.7 PSU	Salinity at the ocean floor

GMDD
8, 9859–9924, 2015

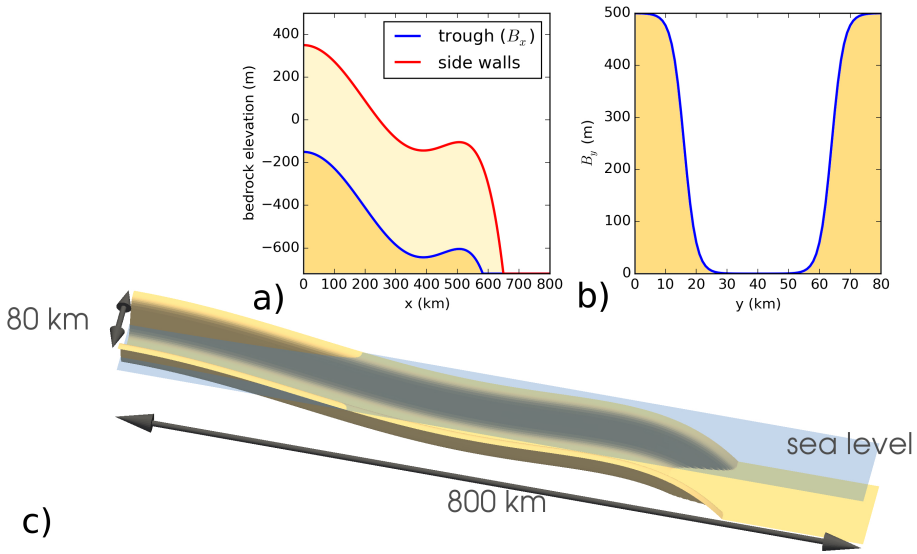

Figure 1. The bedrock topography for the three MIPs as defined by Eqs. (1)–(4). **(a)** $B_x(x)$, the variability of the bedrock topogrpahy in the x direction. The topography through the central trough is shown in blue and on the side walls is shown in red. **(b)** $B_y(y)$, the bedrock topography in the y driection relative to that at the center of the trough. **(c)** The topography in 3-D at 1 km resolution. Sea level is shown in translucent blue.

GMDD
8, 9859–9924, 2015

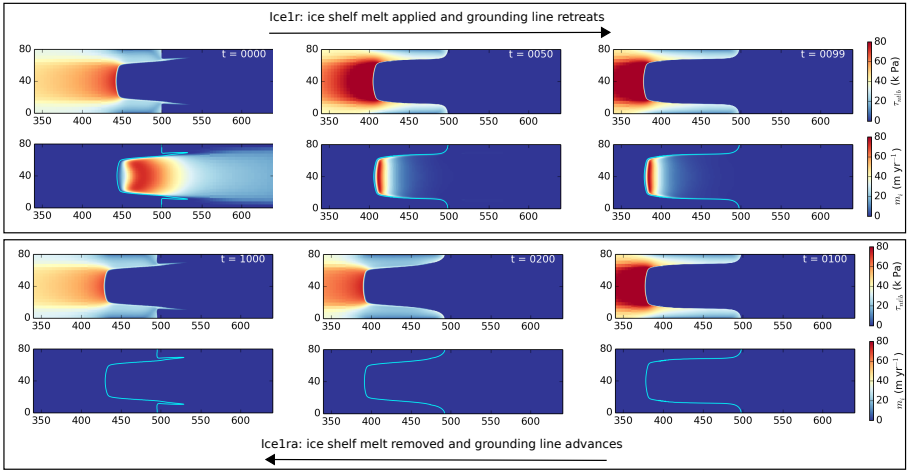

Figure 2. Evolution of the basal traction $\tau_{nt}|_b$ and ice shelf melt rate m_i fields during the Ice1r and Ice1ra experiments from a BISICLES run. Melt rates are applied when $0 < t < 100$ yr, causing the ice shelf to thin and grounding line to advance. Once $t > 100$ yr, no melt is applied, the ice shelf thickens, and the grounding line advances. The choice of the Tsai et al. (2015) traction law ensures that $\tau_{nt}|_b$ is continuous across the grounding line but large ~ 1 km upstream. Similarly, the factor $\tanh\left(H_c/H_{c0}\right)$ ensures that m_i is continuous across the grounding line but large ~ 10 km downstream.

GMDD
8, 9859–9924, 2015

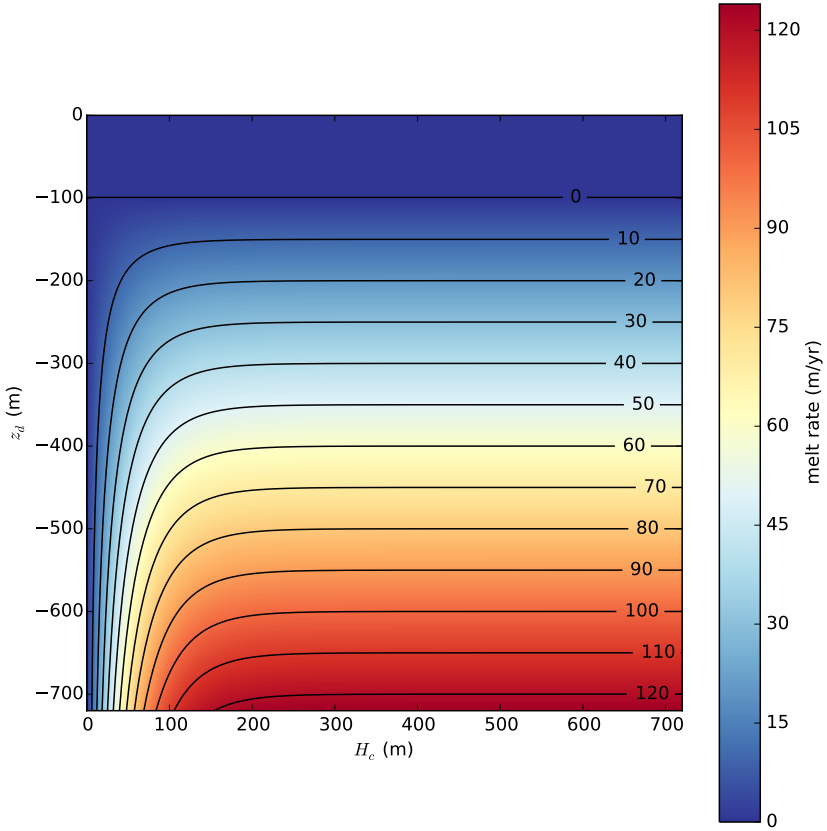

Figure 3. The melt parameterization given by Eq. (14) as a function of the ocean column thickness (H_c) and the ice draft (z_d). Melting increases linearly with decreasing z_d below $z_0 = -100$ m. The melt rate is independent of H_c when H_c is larger than ~ 200 m, but falls to zero as H_c approaches zero.

GMDD
8, 9859–9924, 2015

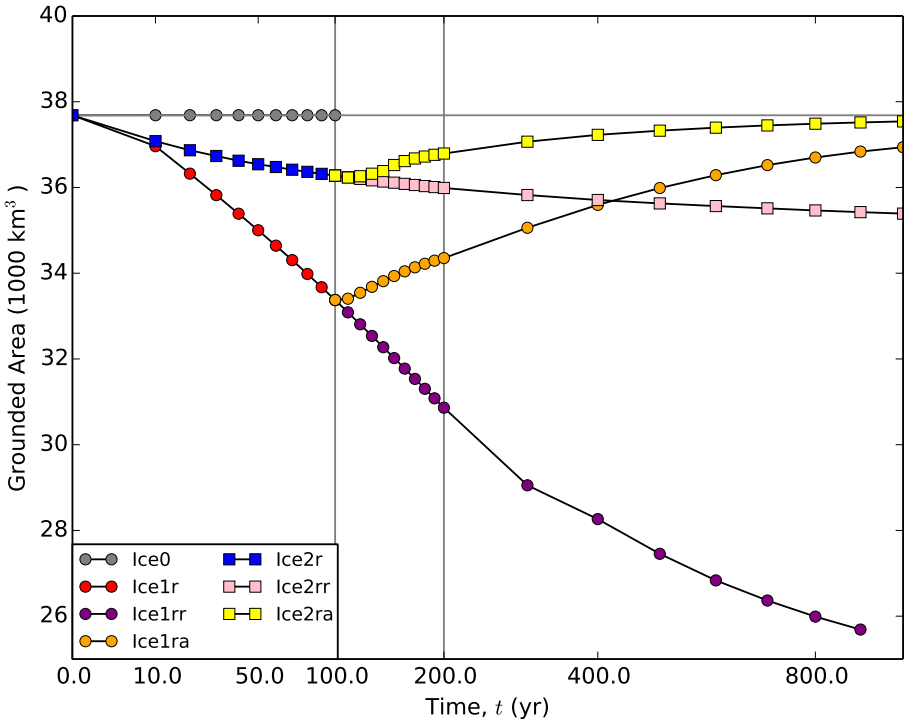

Figure 4. Grounded area plotted against time for the MISMIP+ experiments, computed using BISICLES with the SSA and the Tsai et al. (2015) basal traction. The Ice0, Ice1r and Ice2r experiments all start from steady-state, and apply either zero melt (Ice0) or melt rates derived from simple formulae (Ice1r and Ice2r) from $t = 0$ to $t = 100$ yr. Following on from Ice1r, the Ice1ra and Ice1rr experiments evolve the ice sheet until at least $t = 200$ yr and optionally to $t = 1000$ yr, with the melt rate set to zero in Ice1ra and derived from the same formula as Ice1r in Ice1rr. Ice2ra and Ice2rr follow on from Ice2r in a similar fashion.

GMDD
8, 9859–9924, 2015

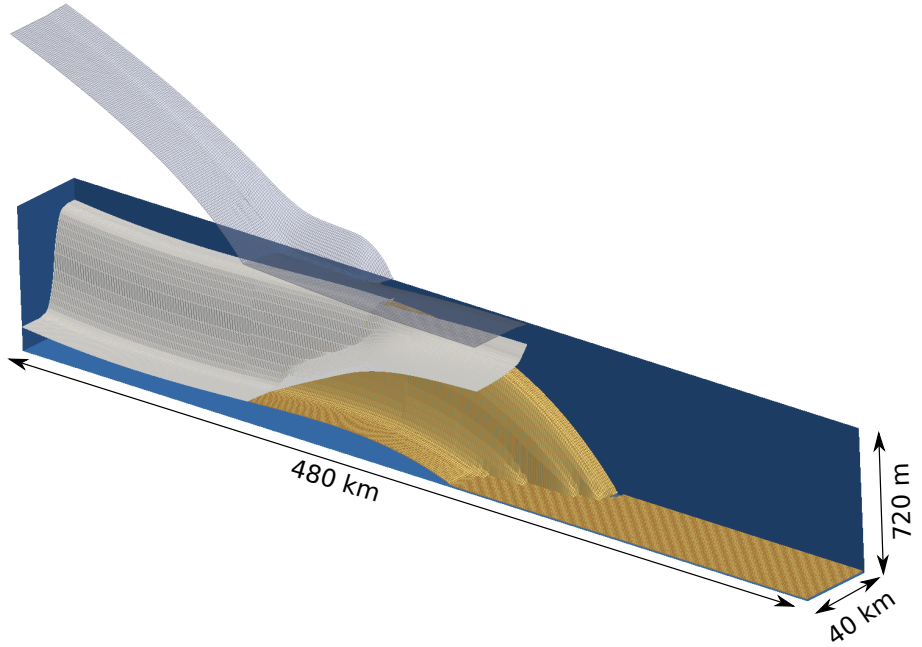

Figure 5. For Ocean1, the surface elevation (translucent blue), ice draft (white) and bathymetry (beige) cut down the center of the trough (y = 40 km) for clearer visualization. The geometry is a steady-state profile from an SSA simulation in BISICLES without basal melting (the initial condition for MISMIP+). The blue walls indicates the bounds of the ocean domain. This geometry is also the starting state of Ocean3.

GMDD
8, 9859–9924, 2015

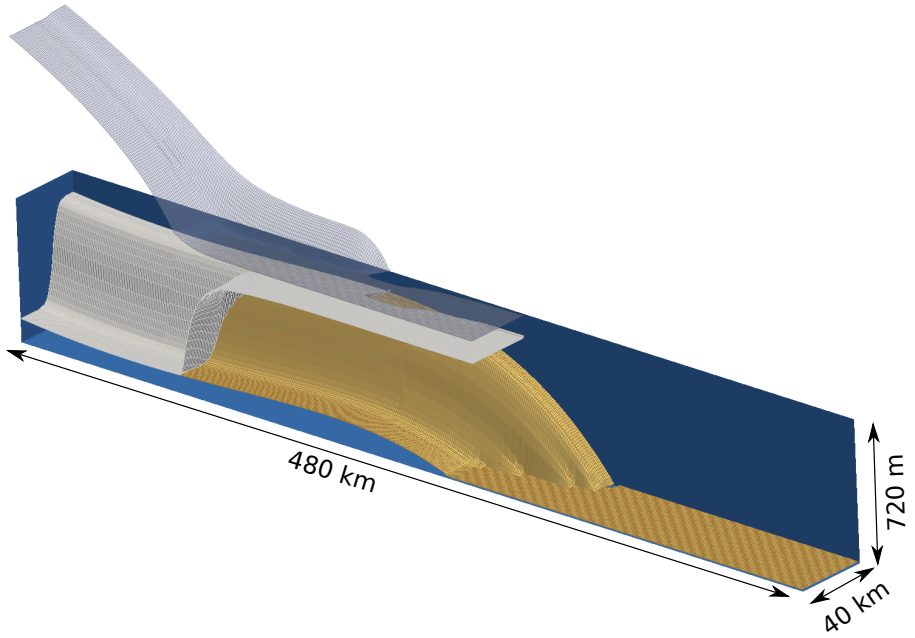

Figure 6. As in Fig. 5 except the geometry for Ocean2. The geometry is from 100 years into a MISMIP+ simulation using BISICLES with the SSA. The geometry is also the final state of Ocean3 and the initial state of Ocean4.

GMDD
8, 9859–9924, 2015

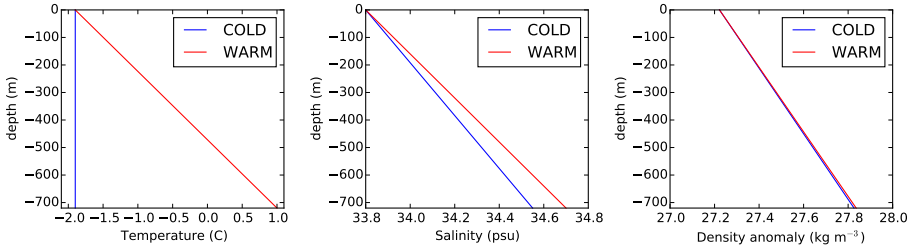

Figure 7. WARM and COLD temperature, salinity and density profiles used in all four ISOMIP+ experiments. In Ocean1, the COLD profile specifies the initial condition and the WARM profile is used in the restoring, while in Ocean2 the profiles are switched. Ocean3 uses both WARM initial conditions and restoring whereas Ocean4 uses both COLD initial conditions and restoring. The WARM profiles were designed to qualitatively approximate observations in the Amundsen Sea Embayment near Pine Island Glacier (Dutrieux et al., 2014). The COLD profile is at the surface freezing temperature at all depths and has a salinity such that the densities of the WARM and COLD profiles are nearly identical.

GMDD
8, 9859–9924, 2015

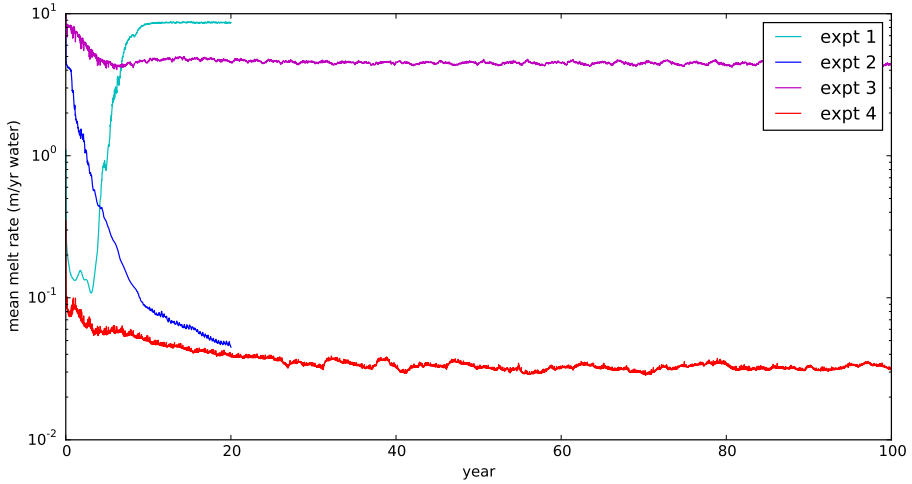

Figure 8. Example results from a POP2x simulation showing the melt rate averaged over the shelf area as a function of time for the four ISOMIP+ experiments. Melting increases by nearly two orders of magnitude in Ocean1, and decreases by about the same order in Ocean2, demonstrating that changes in far-field forcing can greatly increase or reduce melting. After a decade or two of initial adjustment, the melt rates in Ocean3 and Ocean4 remain relatively steady in time despite the changing geometry in those cases, suggesting that the total cavity size has relatively little impact on total melting.

GMDD
8, 9859–9924, 2015

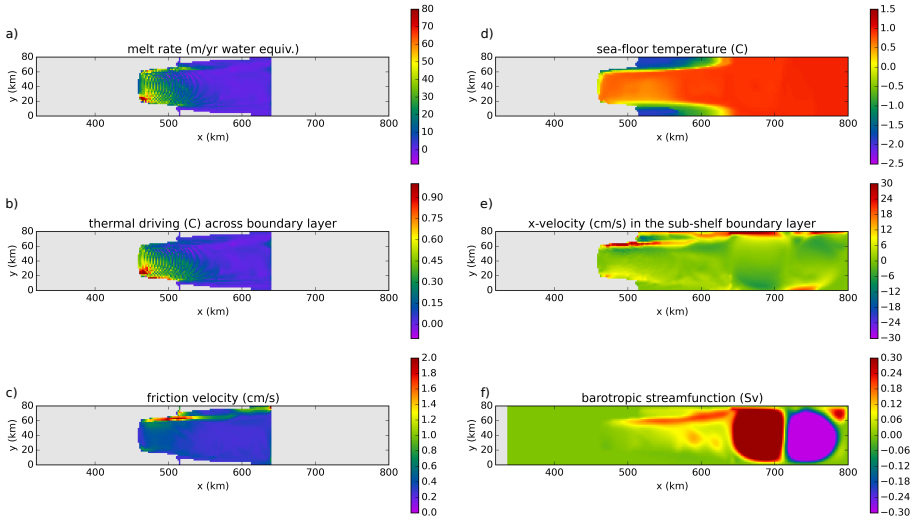

Figure 9. Example results from a POP2x simulation of Ocean1 averaged over the last month of the experiment. **(a)** The melt rate is proportional to the product of **(b)** the thermal driving across the sub-ice-shelf boundary layer and **(c)** the friction velocity. **(d)** The temperature in the bottom-most cell, indicating that warm water has reached the ice-shelf base. **(e)** The x component of the boundary-layer velocity shows a strong jet along the western boundary of the cavity. **(f)** The barotropic streamfunction shows two counter-rotating cells covering the open-ocean region and a weaker clockwise circulation on the western flank of the ice-shelf cavity.

GMDD
8, 9859–9924, 2015

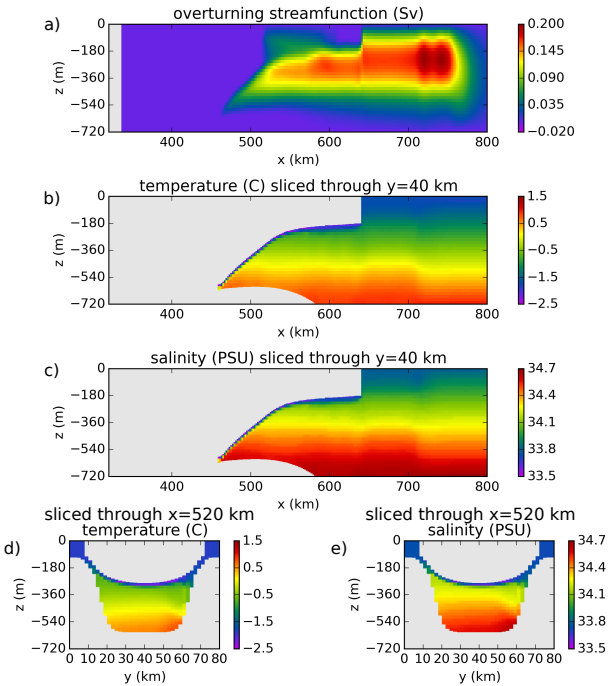

Figure 10. Further example results from the last month of a POP2x simulation of Ocean1. **(a)** The overturning streamfunction shows inflow at depth and outflow at the surface within the cavity. A weaker overturning also occurs in the areas of open ocean on the sides of the ice tongue between x = 500 and 600 km. **(b, c)** Slices of temperature and salinity in an x–z plane through the center of the domain show cold, fresh melt water near the ice–ocean interface. **(d, e)** Slices of temperature and salinity in a y–z planes looking south into the cavity show a slightly thicker melt plume on the western (right) flank.

GMDD
8, 9859–9924, 2015

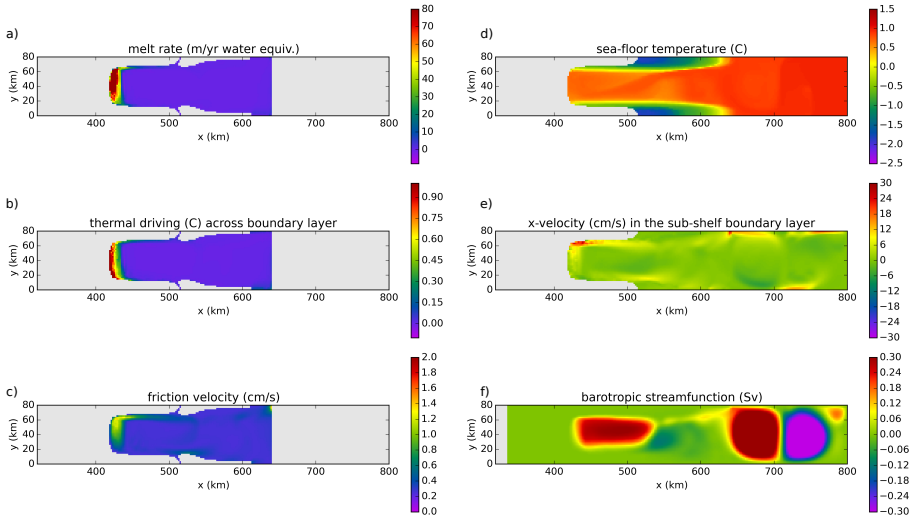

Figure 11. As in Fig. 9 but averaged over the last month of Ocean3. The ice-shelf has retreated and calved significantly, leading to large melt rates concentrated near the grounding line. The jet of melt water visible in **(c, d)** in Fig. 9 is not as strong here, presumably because of the shallower ice draft over most of the cavity. The barotropic circulation is strong in the cavity but weaker in the open ocean than in Ocean1.

GMDD
8, 9859–9924, 2015

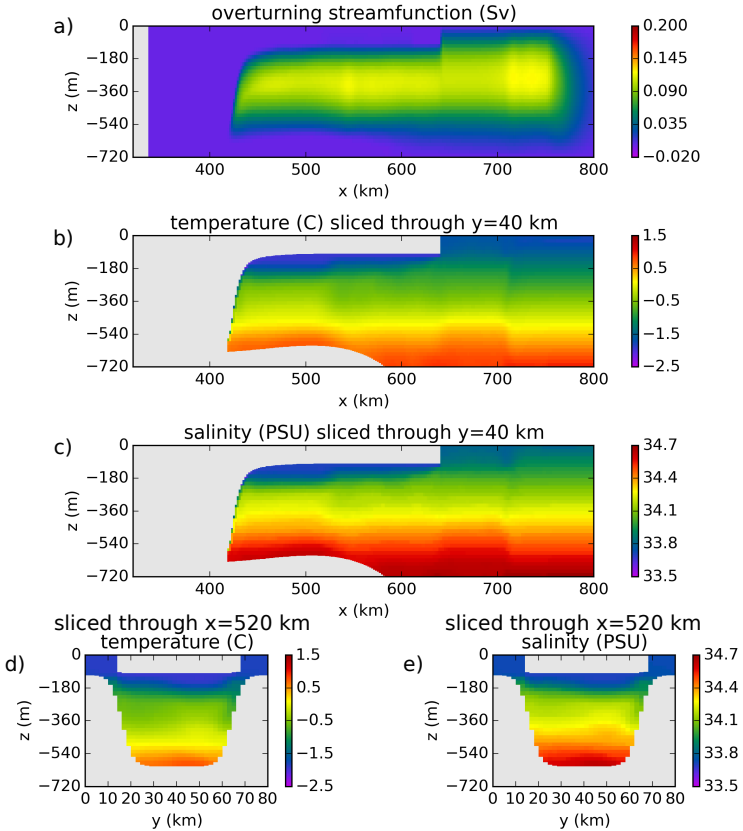

Figure 12. As in Fig. 10 but averaged over the last month of Ocean3. The overturning is somewhat weaker than in Ocean1, perhaps due to the weaker average melting or the relatively flat ice draft over most of the cavity. The melt plume appears to be significantly thicker than in Ocean1, presumably as a result of the shallower ice draft and cooler ambient water in much of the cavity.

GMDD
8, 9859–9924, 2015

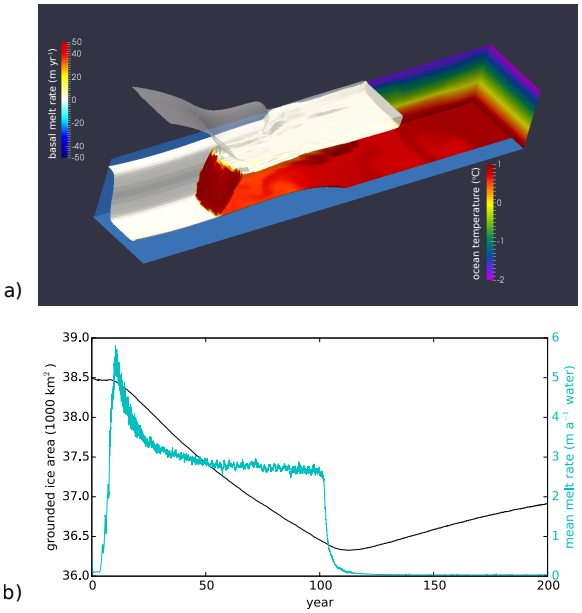

Figure 13. Results from a POPSICLES simulation of IceOcean1. **(a)** The ice topography taken from 100 years with the eastern 20 km of the domain cut away to reveal the behavior within the trough. The basal melt rate is plotted on the ice draft and the ocean temperature is plotted on the bedrock topography and the side walls. The ice-shelf has retreated several tens of kilometers and the ice draft has steepened significantly, leading to large melt rates concentrated near the grounding line, as in Ocean3. **(b)** The grounded area of ice (left axis) and melt rate averaged over the ice-shelf base (right axis) for the 200 year duration of the IceOcean1 experiment. The change in grounded area is less than in the Ice1 results from Fig. 2. As in Ocean1, the mean melt rate increases significantly as warm water first reaches the cavity. As in Ocean3, the melting tails off past year 10 as the shelf begins to thin, leaving less area exposed to the warmer, deeper waters.

GMDD
8, 9859–9924, 2015